PAIN

Engineered zinc finger repressors induce a prolonged and selective repression of *SCN9A* in nociceptors of nonhuman primates

Mohammad Samie*, Toufan Parman, Mihika Jalan, Jisoo Lee, Patrick Dunn, Jason Eshleman, Dianna Baldwin Vidales, Kenneth Kennard, Josh Holter, Brian Jones, Yonghua Pan, Marina Falaleeva, Sarah Hinkley, Alicia Goodwin, Tammy Chen, Sumita Bhardwaj, Alex Ward, Michael Trias, Anthony Chikere, Madhura Som, Yanmei Lu, Sandeep Yadav, Jason Fontenot, Bryan Zeitler, Amy Pooler†, Kathleen Meyer†

Peripheral neuropathies are estimated to affect several million patients in the US, with no long-lasting therapy currently available. In humans, the Nav1.7 sodium channel, encoded by the *SCN9A* gene, is involved in a spectrum of inherited neuropathies and has emerged as a promising target for analgesic drug development. The development of a selective Nav1.7 inhibitor has been challenging, in part because of structural similarities with other Nav channels. Here, we present preclinical studies for a genomic medicine approach using engineered zinc finger repressors (ZFRs) specifically targeting the human/nonhuman primate (NHP) *SCN9A* gene. Adeno-associated virus (AAV)–mediated delivery of ZFRs in human induced pluripotent stem cell (iPSC)–derived neurons resulted in the reduction of *SCN9A* with no detectable off-target activity. In the spared nerve injury (SNI) neuropathic pain mouse model, AAV-ZFR administration resulted in ≤70% repression of *Scn9a* in mouse dorsal root ganglia (DRGs) and was associated with reduction in pain hypersensitivity. AAV9-mediated intrathecal-lumbar (IT-lumbar) delivery of ZFRs in NHPs demonstrated repression of *SCN9A* in bulk DRG tissue and single-cell levels in nociceptors 1 month after treatment. A lead AAV9-ZFR investigational product, ST-503, was developed and further evaluated in a 6-month study in NHPs. ST-503 administration by IT-lumbar infusion resulted in 50% repression of *SCN9A* in bulk DRG tissue at 6 months without findings of dose-limiting toxicity or impact on neurological and cardiac safety pharmacology. Together, our results support further development of an AAV-delivered ZFR as a potential therapy for patients with peripheral neuropathies.

INTRODUCTION

Peripheral neuropathy, a common chronic pain condition, is recognized as one of the most difficult pain syndromes to manage (*1*, *2*). It results from direct damage to somatosensory neurons (*3*), and it may manifest in numerous ways including small fiber neuropathy, diabetic peripheral neuropathy, trigeminal neuralgia, and postherpetic neuralgia. These conditions, all of which are characterized by severe damage to peripheral neurons, are estimated to affect several million patients in the US (*4*). Patients with peripheral neuropathies are usually refractory to common pain medications. Given the high unmet need and lack of durable treatment options, there is an urgent need to develop long-lasting therapeutics for treatment of chronic peripheral neuropathies.

Nerve injury activates a population of primary afferent sensory neurons called nociceptors, which are responsible for translating noxious stimuli into electrical signals. These signals, in the form of action potentials, are then transmitted from the periphery to the cortex, where the brain can perceive the signal as pain (*5*). Voltage-gated sodium channels (Nav channels) are responsible for initiating and propagating the action potential to the brain and are synthesized in the somata of nociceptors (*6*). The soma resides in the dorsal root ganglia (DRGs) located close to the intervertebral foramina at the cervical, thoracic, lumbar, and sacral spinal cord levels. Nav channels are major molecular regulators of neuronal excitability and are widely expressed in the central and peripheral nervous systems and in cardiac and skeletal muscles. To date, nine different Nav channels (Nav1.1 to Nav1.9) have been identified (*7*, *8*). Of the nine known Nav channels in humans, Nav1.7, Nav1.8, and Nav1.9 have been found to be principally expressed in nociceptors and are known to be associated with pain (*6*). Among these, Nav1.7 is involved in a spectrum of inherited human pain disorders (*9*). Gain-of-function mutations in the *SCN9A* gene that encodes for Nav1.7 have been linked to pain in inherited erythromelalgia (IEM) (*10*, *11*) and paroxysmal extreme pain disorder (PEPD), where patients exhibit a severe excessive pain phenotype (*12*). Alternatively, loss-of-function mutations in *SCN9A* are associated with a clinical condition called congenital insensitivity to pain (CIP), in which individuals exhibit complete loss of pain sensation (*13*). Further studies have shown that Nav1.7 defines the threshold of the action potential and amplifies small depolarizing inputs, acting as the major molecular regulator of signal transduction in nociceptive neurons (*14*, *15*), thus having an essential and nonredundant role in transduction and transmission of pain signaling after noxious stimuli (*16*). Patients with CIP do not display motor, cognitive, sympathetic, or gastrointestinal deficiencies, and except for the loss of pain sensation and, in some cases, anosmia, they generally exhibit normal sensory functions (*13*, *17*). This strongly suggests that Nav1.7 is predominantly involved in pain sensation and establishes Nav1.7 as a promising target candidate for analgesic drug development. The development of selective Nav1.7 small-molecule inhibitors, however, has been challenging. This is primarily due to

Sangamo Therapeutics Inc., Richmond, CA 94804, USA.
*Corresponding author. Email: msamie@sangamo.com
†These authors contributed equally to this work.

similarities in protein sequence and structure of the ligand binding sites among various Nav channels (*7*). Several inhibitors that exhibited selectivity in preclinical studies failed in the clinic because of lack of effect or associated side effects related to cross-reactivity with other Nav channels. For example, PF-05089771 showed selectivity in vitro but did not meet clinical end points in individuals with painful diabetic peripheral neuropathy (*18*). GDC-0276 was never evaluated in patients with neuropathic pain, but at high doses in healthy volunteers, its tolerability was limited because of hypertension and increase in liver enzymes (*19*). Hypertension was also observed with MK-2075, suggesting a possible on-target effect on Nav1.7 expressed in autonomic neurons. This finding could potentially indicate that more restricted biodistribution is required, in addition to specificity, to avoid unwanted side effects.

Zinc fingers (ZFs) are naturally occurring transcription factor proteins that have primarily evolved to regulate eukaryotic gene expression epigenetically and represent the most abundant and diverse class of DNA binding proteins in the human genome (*20*). Over the past several years, zinc finger repressors (ZFRs) were used to repress the expression of different genes involved in various neurological disorders in different preclinical models including chronic pain (*21*), Huntington's disease (*22*), and Alzheimer's disease (*23*). Access to deeper ZF archives has enabled the engineering of large ZFR libraries, facilitating the identification of very selective and potent ZFRs targeting any gene, including *SCN9A*. ZFRs hold several advantages over other genomic medicine approaches; they do not nick or induce double-strand breaks in endogenous genomic DNA, and their components are of human origin, minimizing immunogenicity risk in patients. Furthermore, consistent with their dominant role as part of ~350 different native human Krüppel-associated box (KRAB) proteins, ZFRs often outperform bacterially sourced CRISPR formats in epigenetic transcriptional modulation of human genes (*21*, *24*) and, because they are native to the human body, ZFRs are expected to be generally well tolerated in patients. In addition, the compact size of ZFRs allows for unrestricted packaging into adeno-associated virus (AAV) vectors, thereby enabling the generation of efficient, specific, and long-lasting down-regulation of *SCN9A* expression through a single administration.

Here, we show that a ZFR targeting mouse *Scn9a* was able to induce efficient and fast pain recovery in the mouse neuropathic pain model. A ZFR targeting human/nonhuman primate (NHP) *SCN9A* led to potent and selective repression of *SCN9A* and reduction in heat-mediated neuronal activity in induced pluripotent stem cell (iPSC)–derived human neurons in vitro. The pharmacology and safety of the lead ZFR were investigated in cynomolgus monkeys, where results showed a persistent repression of *SCN9A* for up to 6 months, without dose-limiting toxicity or cardiac issues, illustrating the durability and safety of the approach in NHPs.

RESULTS

NHP/human *SCN9A* targeting ZFR selectively reduce human *SCN9A* and Nav1.7 function in iPSC-derived neurons without altering the expression of other Nav channels

Considering the central role of Nav1.7 in transmitting pain signals to the brain, we hypothesized that reducing Nav1.7 by selective repression of the *SCN9A* gene using ZFRs would reduce the expression of Nav1.7 in neurons and thereby reduce neuropathic pain in peripheral neuropathies. ZFRs are engineered by combining a designed ZF array with a KRAB domain (*25*). The ZF array mediates site-specific binding to the *SCN9A* gene, and the KRAB domain represses the endogenous expression of the *SCN9A* transcript, leading to a reduction in Nav1.7 protein (Fig. 1A).

To identify potent and specific ZFRs, we assembled a library containing several hundred ZFRs targeting conserved sequences between humans and NHPs located on the *SCN9A* transcription start site (TSS) near *SCN9A* exon 1 on chromosome 12 (Fig. 1B). The screening of ZFRs was performed in the SK-N-MC human neuroepithelial cell line using ZFR mRNA nucleofection. SK-N-MC cells express *SCN9A* transcripts and are thus appropriate for testing ZFRs that reduce *SCN9A* expression. Some ZFRs failed to decrease the *SCN9A* transcript, whereas others exhibited a potent repression of the *SNC9A* transcript, with more than 90% repression (Fig. 1B). On the basis of repression profiles, several ZFRs were selected for further evaluation in iPSC-derived γ-aminobutyric acid–producing (GABAergic) neurons. AAV6 has exhibited the greatest ability to transduce a wide range of primary cells in culture compared with other serotypes (*26*); thus, AAV6 was used for the in vitro characterization of ZFRs in neurons. AAV6-mediated delivery of ZFR-1 and ZFR-2 (hereafter referred to as hZFR) yielded a repression of *SCN9A* mRNA in iPSC-derived GABAergic neurons (Fig. 1C), with minimal effect on the expression of the housekeeping gene *ATP5B* (fig. S1A), demonstrating that the ZFRs can potently reduce *SCN9A* transcripts in iPSC-derived neurons in vitro.

To evaluate the potential ZFR off-target impact on global gene expression, a microarray analysis was conducted on total RNA isolated from human iPSC-derived GABAergic neurons transduced with ZFRs. During the course of this study, cells were not stimulated, so downstream effectors of Nav1.7 activation were not evaluated. Three weeks after transduction with a 1×10^5 multiplicity of infection (MOI) of ZFRs packaged into AAV6 vectors, cells were harvested and analyzed using human Clariom S microarrays. The Clariom S microarray contains probes targeting more than 21,000 genes. In addition to *SCN9A*, ZFR-1 differentially regulated the expression of 80 other genes, indicating that ZFR-1 binds near the TSS of those genes. In contrast, hZFR specifically repressed the expression of *SCN9A* mRNA and did not regulate the expression of any other genes in iPSC-derived neurons (Fig. 1D), illustrating that hZFR modules have a high binding specificity for the sequence near the SC*N9A* TSS. hZFR was further characterized in iPSC-derived sensory neurons (which are the target neuronal population for neuropathic pain treatment). AAV6-mediated transduction of hZFR in sensory neurons resulted in potent and dose-dependent repression of *SCN9A* 10 days after transduction (Fig. 1E), with no effect on expression of the housekeeping gene *ATP5B* (fig. S1B). Furthermore, the expression of other Nav channels in iPSC-derived sensory neurons was evaluated after transduction with high hZFR doses using reverse transcription quantitative polymerase chain reaction (RT-qPCR) probes designed specifically for each Nav channel. hZFR potently repressed *SCN9A* with no effect on expression of other Nav channels in iPSC-derived sensory neurons (Fig. 1F).

We evaluated neuronal excitability in response to noxious heat using microelectrode array (MEA) recordings in iPSC-derived sensory neurons obtained from a healthy individual and a patient with IEM. The gain-of-function mutation in Nav1.7 (V400M) present in neurons from patients with IEM causes a voltage-dependent hyperpolarizing shift that leads to an increase in channel excitability and higher firing rate in these cells (*27*). We hypothesized that if hZFR-mediated repression of

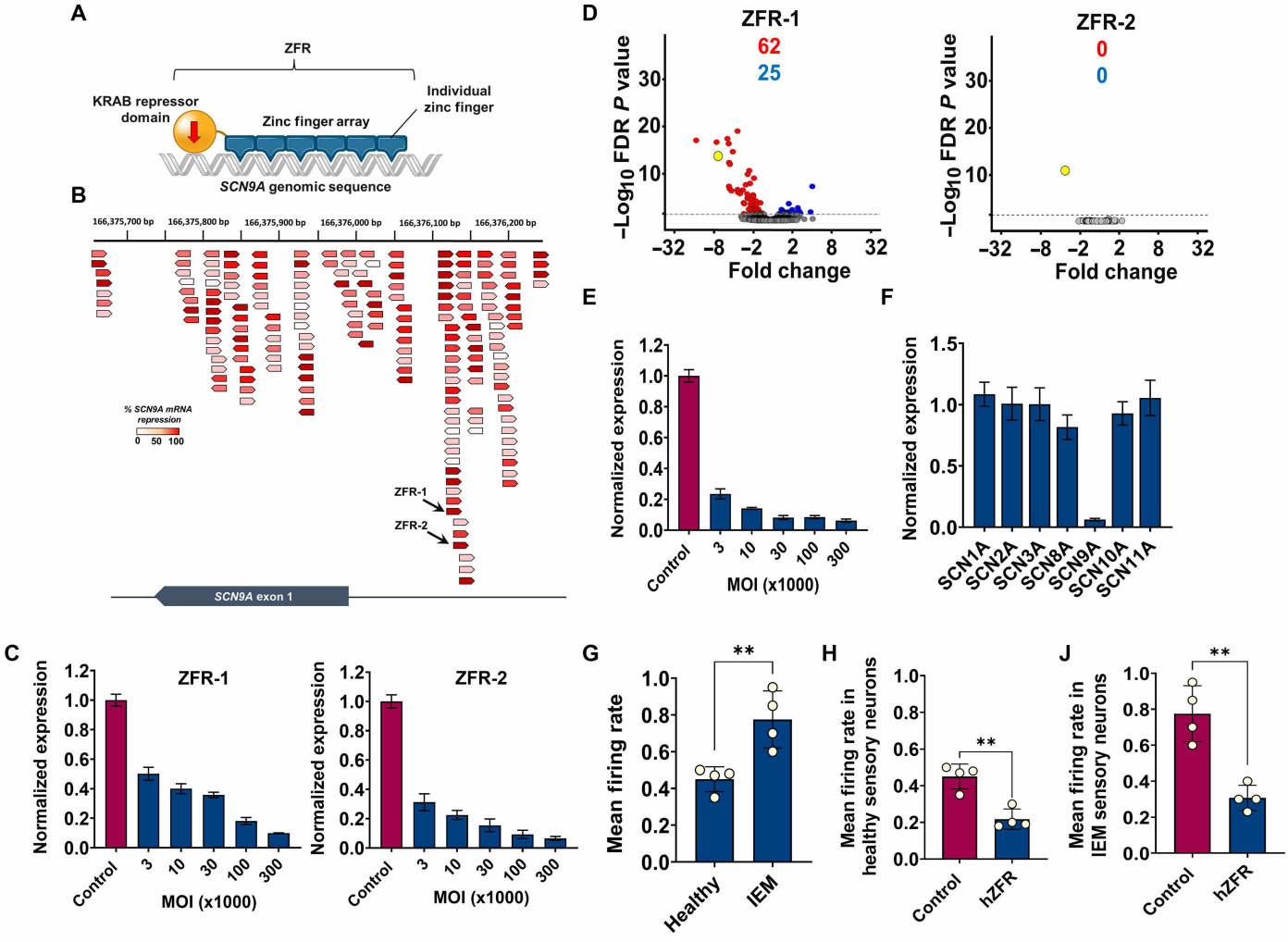

Fig. 1. *SCN9A* targeting hZFR specifically reduces human *SCN9A* and Nav1.7 function in iPSC-derived neurons without influencing the expression of other Nav channels in vitro. (**A**) Engineered ZFRs consist of two main domains: a designed zinc finger array domain, which is specifically binding to the *SCN9A* genomic sequence, and a KRAB transcriptional repressor domain from the human KOX1 protein. The ZFR selectively binds to near the *SCN9A* transcription start site, recruits the KAP1 epigenetic modification complex by the KRAB domain, and represses the expression of *SCN9A*. (**B**) Schematic of binding locations around the human *SCN9A* TSS and the percentage of *SCN9A* mRNA repression of 200 ZFRs tested in SK-N-MC cells. Each arrow indicates a ZFR and its orientation (sense or antisense) regarding *SCN9A* exon 1. The heatmap (red-white) illustrates *SCN9A* expression levels after ZFR treatment. The arrow color indicates % *SCN9A* repression; white represents no repression of *SCN9A*. The numbers on top represent the genomic location on chromosome 12. bp, base pairs. (**C**) Normalized *SCN9A* expression in iPSC-derived GABAergic neurons after AAV6-mediated transduction of ZFR-1 or hZFR. Doses (MOI): 3×10^3, 1×10^4, 1×10^5, and 3×10^5. Means ± SD. Control group is cells treated with another AAV-ZFR that does not target *SCN9A* and targets another gene (see Materials and Methods). (**D**) mRNA microarray assessment (volcano plots) of iPSC-derived GABAergic neurons 30 days after AAV6-mediated transduction of ZFR-1 or hZFR (delivered to cells at 1×10^5 MOI). Each dot represents the mean fold change compared with control-treated cells for a given gene (*x* value) and the associated *P* value (*y* value). Gene expression profiles were calculated on the basis of false discovery rate (FDR)–adjusted *P* value > 0.05. Red dots represent genes that are down-regulated, blue dots represent genes that are up-regulated, and yellow dot indicates the *SCN9A* gene. Six biological replicates. (**E**) Normalized *SCN9A* expression in iPSC-derived sensory neurons 7 days after AAV6-mediated transduction of hZFR. Doses (MOI): 3×10^3, 1×10^4, 3×10^4, 1×10^5, and 3×10^5. Means ± SD. Control is a ZFR that does not target *SCN9A*. (**F**) Normalized expression of Nav channels 7 days after AAV6-mediated transduction of hZFR (at 3×10^5 MOI). Means ± SD. (**G**) Heat-induced neuronal mean firing rate in iPSC-derived sensory neurons isolated from healthy individuals or patients with IEM. Each circle represents an independent reading from 500 neurons. Means ± SD. (**H** and **I**) Heat-induced neuronal mean firing rate in iPSC-derived sensory neurons isolated from healthy individuals or patients with IEM after hZFR treatment. Each circle represents an independent reading from 500 neurons. Means ± SD. Control is a ZFR that does not target *SCN9A*.

SNC9A transcripts leads to repression of Nav1.7 protein, we should see a functional decrease in neuronal hyperexcitability in response to heat stimulation in neurons isolated from patients with IEM. iPSC-derived sensory cells from healthy individuals or patients with IEM expressed the neuronal marker Tuj1 after differentiation (fig. S2). We then measured neuronal firing in response to heat using the MEA system to quantify the excitability of healthy and IEM neurons after hZFR treatment. IEM cells exhibited higher firing rates compared with healthy sensory neurons after heat activation (Fig. 1G) as reported previously (*27*). One week after AAV6-hZFR treatment, a twofold decrease in average firing rate was observed in iPSC-derived sensory neurons from healthy donors and patients with IEM (Fig. 1, H to J). Together, data obtained from iPSC-derived neurons indicate that hZFR potently and selectively targets *SCN9A* and reduces Nav1.7 function in vitro.

Repression of *Scn9a* in the spared nerve injury mouse model of neuropathic pain reverses pain hypersensitivity

Because the target genome sequences encoding the Nav1.7 sodium channel differ between mouse *Scn9A* and NHP/human *SCN9A*, surrogate mZFRs were generated to demonstrate the effectiveness of ZFRs in vivo in a mouse neuropathic pain model. Before testing in vivo, mZFRs were screened in a mouse Neuro2A (N2A) neural crest–derived cell line. The lead mZFR with potent repression (fig. S3A) was selected for further analysis in neurons isolated from mouse DRGs. The lead mZFR was selective toward *Scn9a* and did not influence expression of other Nav channels expressed in DRG neurons (fig. S3B). In addition, 1 week after transduction, a reduction in mean neuronal firing was observed after heat activation, confirming the reduction of Nav1.7 functionality in DRG neurons (fig. S3C).

Before conducting pain assessment studies, the on-target activity of AAV9-mediated delivery of mZFR (AAV9-mZFR) was evaluated in lumbar DRGs of C57BL/6 mice 4 weeks after a single intrathecal-lumbar (IT-L) administration (Fig. 2A). Like hZFR, mZFR expression was driven by the neuronal-specific human synapsin (Syn) promoter. Although repression of *Scn9a* was observed in bulk lumbar DRGs (Fig. 2B), no statistical up-regulation of the neuroinflammation marker *Iba1* or down-regulation of the neuronal marker *Rbfox3* was observed compared to the vehicle group, demonstrating lack of neuroinflammatory responses or neuronal loss in lumbar DRGs 1 month after AAV9-mZFR administration in mice (Fig. 2, C and D).

The effectiveness of mZFR was evaluated in the spared nerve injury (SNI) mouse model of neuropathic pain (Fig. 2E). Results from this model provide an understanding of the relationship among ZFR expression, *Scn9a* repression, and efficacy in reducing neuropathic pain. The SNI model in rodents is a partial denervation model that involves cutting the common peroneal and tibial nerves while sparing the sural nerve, leading to consistent and reproducible tactile pain hypersensitivity in the skin territory of the spared intact sural nerve (*28*). The SNI model has proven to be robust, demonstrating substantial and prolonged changes in measures of mechanical sensitivity and thermal responsiveness, reminiscent of clinically described conditions for neuropathic pain disorders (*28*). Before surgical procedures, a pain sensitivity baseline was measured for all animals using von Frey filaments for the assessment of mechanical-induced pain (filaments were applied from the underside of the mesh to the surface of the mouse hind paw) and a cold plate for cold-induced pain. Seven days after the SNI surgery and after collection of a baseline responses of the mouse model to mechanical- and cold-induced pain, mice (eight males and eight females) were assigned to their respective groups, and a single IT-L dose of either vehicle or AAV9-mZFR at 8×10^{11} vector genomes (vg) per animal was administered into the L4-L5 intervertebral space. For the sham (control) group, animals underwent surgery, but nerves were not cut (only skin opened and sutured closed) and AAV9-mZFRs were not administered. One month after dosing, animals were euthanized, and DRGs were collected and evaluated for expression of *Scn9a* at the bulk and single-cell levels. Mechanical- and cold-induced pain were measured during the course of the study to assess efficacy of mZFR (Fig. 2E). In addition, clinical observations, body weights, and necropsy observations were performed to assess tolerability. Bulk DRG analysis using RT-qPCR demonstrated ~70% reduction in *Scn9a* expression in lumbar and cervical DRG levels compared with ~40% repression in thoracic DRGs in both male and female animals (Fig. 2F). There were no gender differences in terms of *Scn9a* repression. RNAscope in situ hybridization (ISH) was used in combination with immunohistochemistry (IHC) to assess *Scn9a* mRNA repression on a single-cell level. The nociceptors were identified with a peripherin-specific antibody (green). *Scn9a* mRNA was observed in peripherin+ cells in lumbar DRGs isolated from the vehicle group. Reduction of the *Scn9a* mRNA (white) transcript was observed in peripherin+ cells in AAV9-mZFR–treated animals (Fig. 2G), illustrating that mZFR was able to reduce the expression of the *Scn9a* transcript in mouse nociceptors.

Mechanical- and cold-induced pain were measured predose before SNI surgery to establish a baseline (Fig. 3, A and B). Before dose administration (7 days after SNI surgery), mechanical- and cold-induced pain were measured again to establish baseline. All mice that underwent SNI surgery demonstrated lower mechanical- and cold-induced pain thresholds compared with the sham control group. This was made evident by mice responding to less force than necessary to the affected limb to elicit a withdrawal behavior or quicker paw withdrawal from the cold plate as compared with the sham group. Animals treated with a single IT-L dose of AAV9-mZFR demonstrated an increase in mechanical-induced pain threshold compared with their respective vehicle control groups on day 28 (Fig. 3A). On day 28, the mechanical-induced pain threshold in AAV9-mZFR animals was comparable to that of the sham group, indicating that ZFR treatment was able to restore pain responses to normal levels. In addition, to further validate the effectiveness of AAV9-mZFR, a small-molecule analgesic drug, gabapentin (GBP), was included as a positive control. GBP was administered intraperitoneally ~1 hour before testing on day 28. The timing for GBP administration was selected on the basis of its reported time to reach maximum plasma concentration and nociceptive effectiveness. Paw withdrawal latency in response to cold-induced pain increased in AAV9-mZFR–treated animals compared with the vehicle group (Fig. 3B). On day 28, the cold-induced pain threshold in mZFR-treated animals was comparable to that in sham- and GBP-treated animals. The relationship between the degree of pain recovery after mZFR treatment and *Scn9A* repression was evaluated for both mechanical- and cold-induced pain for each individual animal. In lumbar DRGs, 30 to 40% repression of *Scn9a* was sufficient to induce ~50% recovery in mechanical-induced pain (Fig. 3C) and ~75% recovery in cold-induced pain (Fig. 3D). Longitudinal assessment of mechanical- and cold-induced pain responses in female and male animals after AAV9-mZFR treatment revealed that AAV9-mZFR was able to rescue the mechanical-induced pain phenotype as early as 3 days postdose (Fig. 3E) and cold-induced pain as early as 8 days postdose (Fig. 3F) in the SNI neuropathic pain model. The pain threshold gradually increased to similar levels as in sham-treated animals by day 28, demonstrating that mZFR is active within days of treatment in neurons. The expression of neuronal injury markers ATF3 and GAP43 was comparable between vehicle and AAV9-mZFR–treated animals at day 29 (fig. S4, A and B). SmartCage analysis between the hours of 6:00 p.m. and 5:00 a.m. was used to evaluate any possible changes or recovery in animal movement after treatment with AAV9-mZFR. The relevant SmartCage parameters for the SNI mouse model are mean activity time (MAT; measures free movement within the cage) and mean rearing count (MRC; measures number of times animals stand on both hind paws in a vertical upright position). In general, the vehicle group exhibited lower values for MAT and MRC compared with the sham group, which is anticipated because sham animals did not have full SNI surgery (Fig. 3, G and H, and fig. S5, A and B). MAT and MRC values increased in AAV9-mZFR–treated animals compared with the

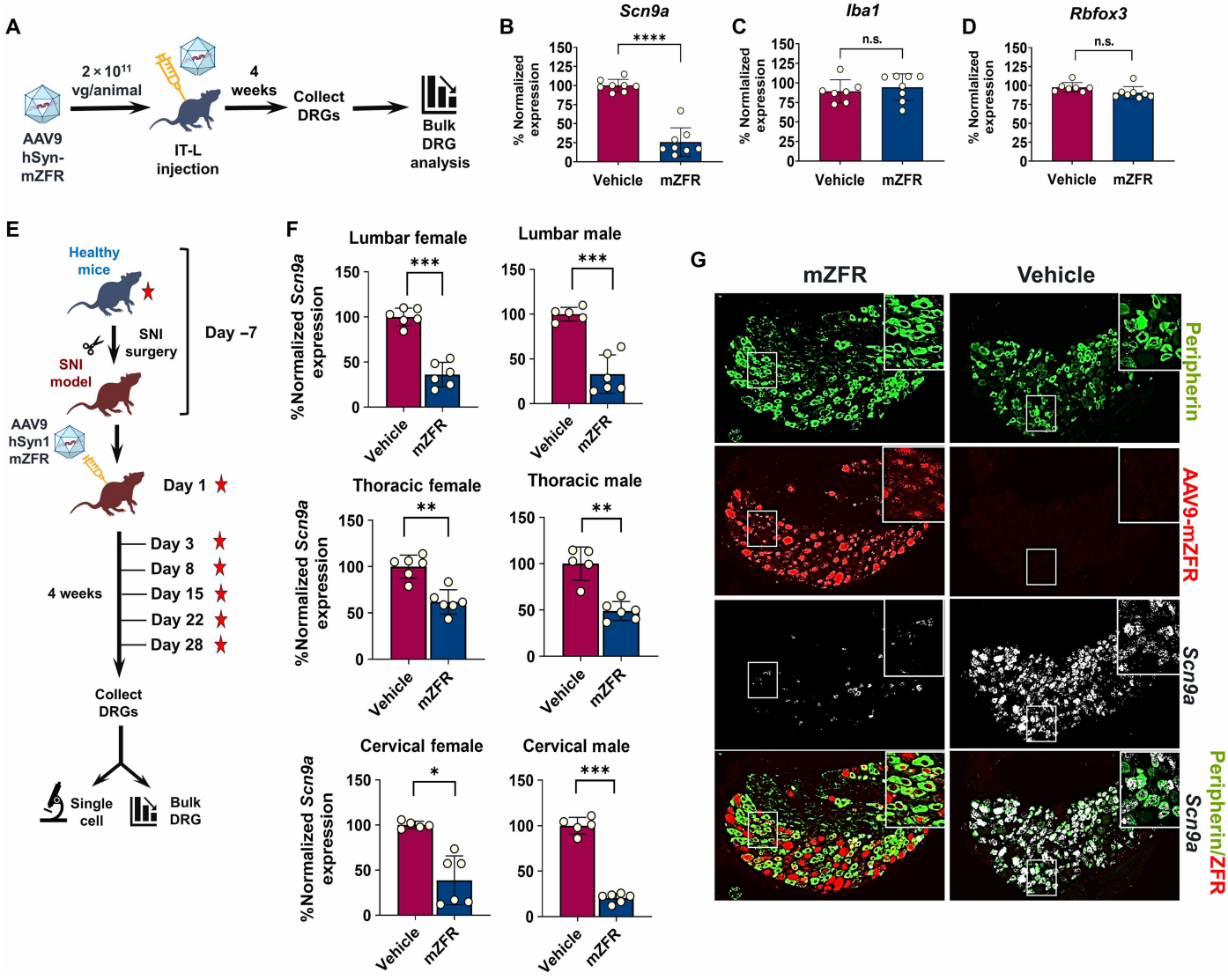

Fig. 2. ZFR-mediated repression of *Scn9a* in a mouse model of neuropathic pain. (**A**) Overview and timeline of the target engagement and tolerability study in wild-type (WT) mice using mZFR packed into AAV9. (**B**) Normalized mRNA expression of *Scn9a* in lumbar DRGs 4 weeks after IT-L injection compared with the vehicle group. Means ± SEM. (**C**) Normalized mRNA expression of *Iba1* (a microglia-mediated neuroinflammatory marker) in the lumbar DRGs, 4 weeks after IT-L injection compared with the vehicle group. Means ± SEM. (**D**) Normalized mRNA expression of *Rbfox3* (neuronal marker) in the lumbar DRGs, 4 weeks after IT-L injection compared with the vehicle group. Means ± SEM. (**E**) Overview and timeline of the pain efficacy study using the SNI mouse model. Red stars indicate the time points where pain responses were measured. Mechanical and cold allodynia were measured in WT mice before they underwent SNI surgery. Seven days after the SNI surgery (day 1), mechanical and cold allodynia were measured again, and animals were injected with AAV9-hSyn1-mZFR at 8×10^{11} vg per animal. Pain responses were measured at different time points postinjection (days 3, 8, 15, 22, and 28). After 4 weeks, animals were euthanized and DRGs were collected for gene expression and pathological analysis. Stars indicate the time points where pain responses were measured. (**F**) Normalized average mRNA expression of *Scn9a* in mouse lumbar, thoracic, and cervical DRGs obtained from female and male animals. Means ± SEM; ordinary one-way ANOVA, $^{**}P < 0.01$; $^{***}P < 0.001$; $^{****}P < 0.0001$ compared with vehicle. (**G**) Representative IHC images of lumbar DRGs from mice injected with AAV9-hSyn1-mZFR or vehicle. Sections were immunolabeled for peripherin [nociceptor marker (green)] and hybridized with fluorescently labeled mouse-specific *Scn9a* and ZFR RNA probes. Scale bars, 50 μm.

vehicle group and were similar to levels in sham group animals for both male and female mice (Fig. 3, G and H, and fig. S5, A and B). MAT and MRC values also increased in AAV9-mZFR–treated animals compared with GBP-treated animals. Together, these data show that in vivo repression of mouse *Scn9a* reversed pain hypersensitivity and improved movement and rearing in an SNI mouse model of neuropathic pain.

AAV9-hZFR induced a specific and dose-dependent repression of *SCN9A* in multiple DRG levels 1 month after IT-L injection in NHPs

Pharmacology and target specificity of AAV9-mediated delivery of hZFR (AAV9-hZFR) were evaluated in cynomolgus monkeys in a 1-month dose range-finding pharmacology and safety study after a single IT-L administration at three dose levels: 1×10^{12}, 1×10^{13},

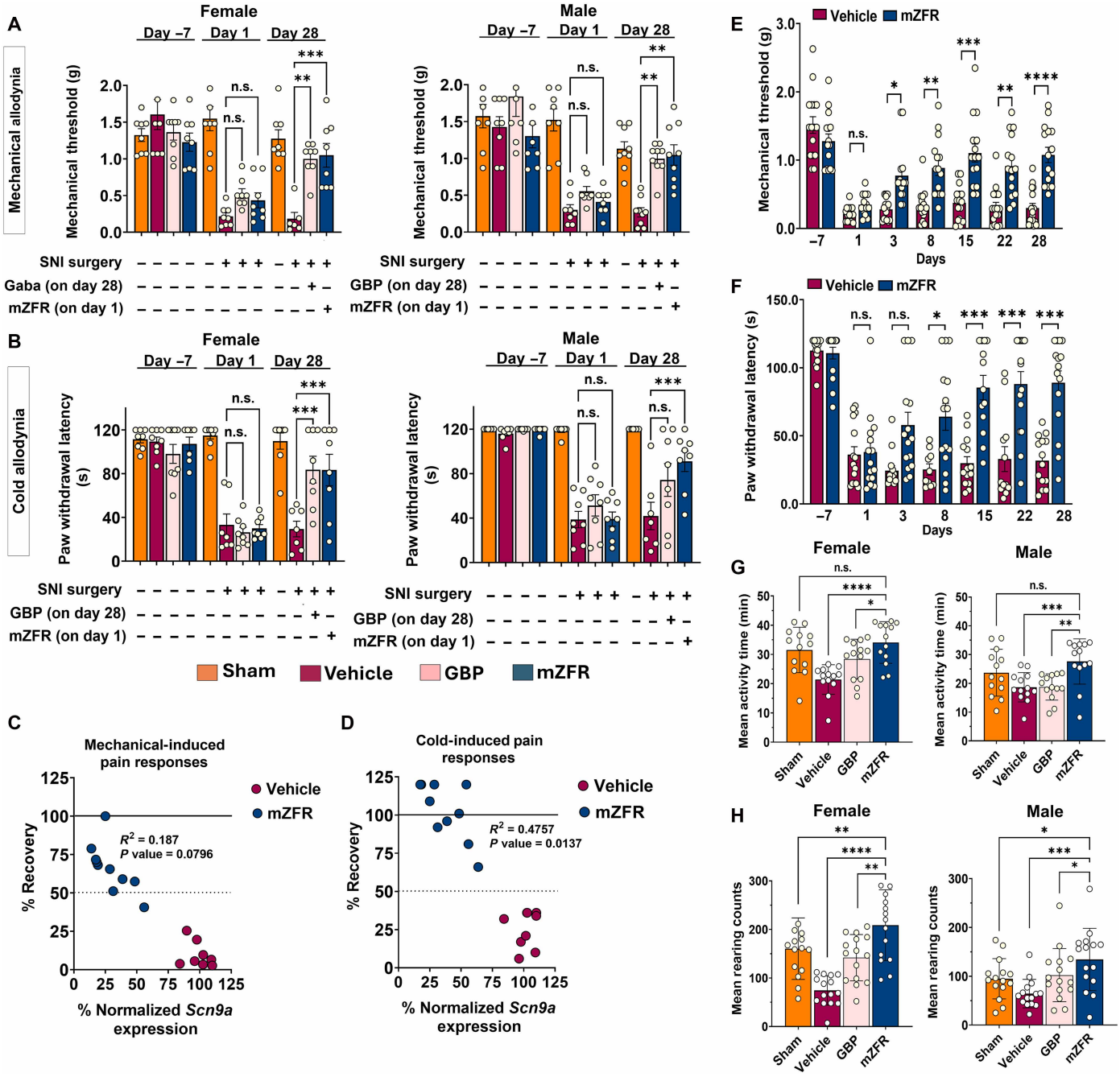

Fig. 3. In vivo repression of *Scn9A* reverses pain hypersensitivity in a mouse model of neuropathic pain without altering overall activity. (**A** and **B**) Mechanical-induced (A) or cold-induced (B) pain responses were measured at day −7 (healthy mice) and at day 1 (7 days after SNI surgery), and, 28 days after AAV9-mZFR IT-L injection in all groups, GBP was injected on day 28, 1 hour before pain measurements. Dots represent individual animals; $n = 7$ or 8. Means ± SEM; one-way ANOVA, $^{**}P < 0.01$; $^{***}P < 0.001$; $^{****}P < 0.0001$ compared with the vehicle group. (**C** and **D**) Relationship between the reduction of *Scn9a* mRNA and the pain response in mice treated with AAV9-mZFR. Degree of behavioral recovery was calculated for both mechanical-induced (C) and cold-induced (D) pain. $N = 12$ (six males and six females) per AAV9-mZFR. *Scn9a* was normalized to housekeeping genes, and % recovery was calculated for each animal as mechanical pain response on day 28 divided by response on day 1, multiplied by 100. Correlation coefficient (R^2) and P values are included for each figure. (**E** and **F**) Daily pain responses for mechanical-induced (E) and cold-induced (F) pain after AAV9-mZFR treatment. Dots represent individual animals; $n = 12$. Means ± SEM; one-way ANOVA, $^{**}P < 0.01$; $^{***}P < 0.001$; $^{****}P < 0.0001$ compared with the vehicle group. (**G** and **H**) SmartCage assessment was performed on SNI mice at day 28 after IT-L injection of AAV9-mZFR. Mean activity time (G) and mean rearing count (H) were evaluated for both male and female animals during the dark cycle. Dots represent a time point in the dark cycle. Means ± SEM; one-way ANOVA, $^{**}P < 0.01$; $^{***}P < 0.001$; $^{****}P < 0.0001$ compared with the vehicle group.

and 9×10^{13} vg per animal (Fig. 4A). Similar to mZFR in mouse studies, hZFR expression was controlled by the neuronal-specific human Syn promoter. The potency of AAV9-hZFR was evaluated at bulk DRG levels (lumbar, thoracic, and cervical) and in nociceptors using RNAscope. AAV9-hZFR was expressed in a dose-dependent manner in all DRG regions analyzed (Fig. 4B) and repressed *SCN9A* expression by 40 to 60% at bulk DRG levels compared with the vehicle group (Fig. 4C). To confirm the specificity of hZFR in vivo, the expression of other known Nav channels in DRGs was evaluated, including Nav1.6 (*SCN8A*), Nav1.8 (*SCN10A*), and Nav1.9 (*SCN11A*), after IT-L administration of AAV9-hZFR. Supporting target specificity, no changes in expression of other Nav channels were observed in DRGs at any dose (Fig. 4D), confirming the in vitro data that hZFR is selective toward *SCN9A*.

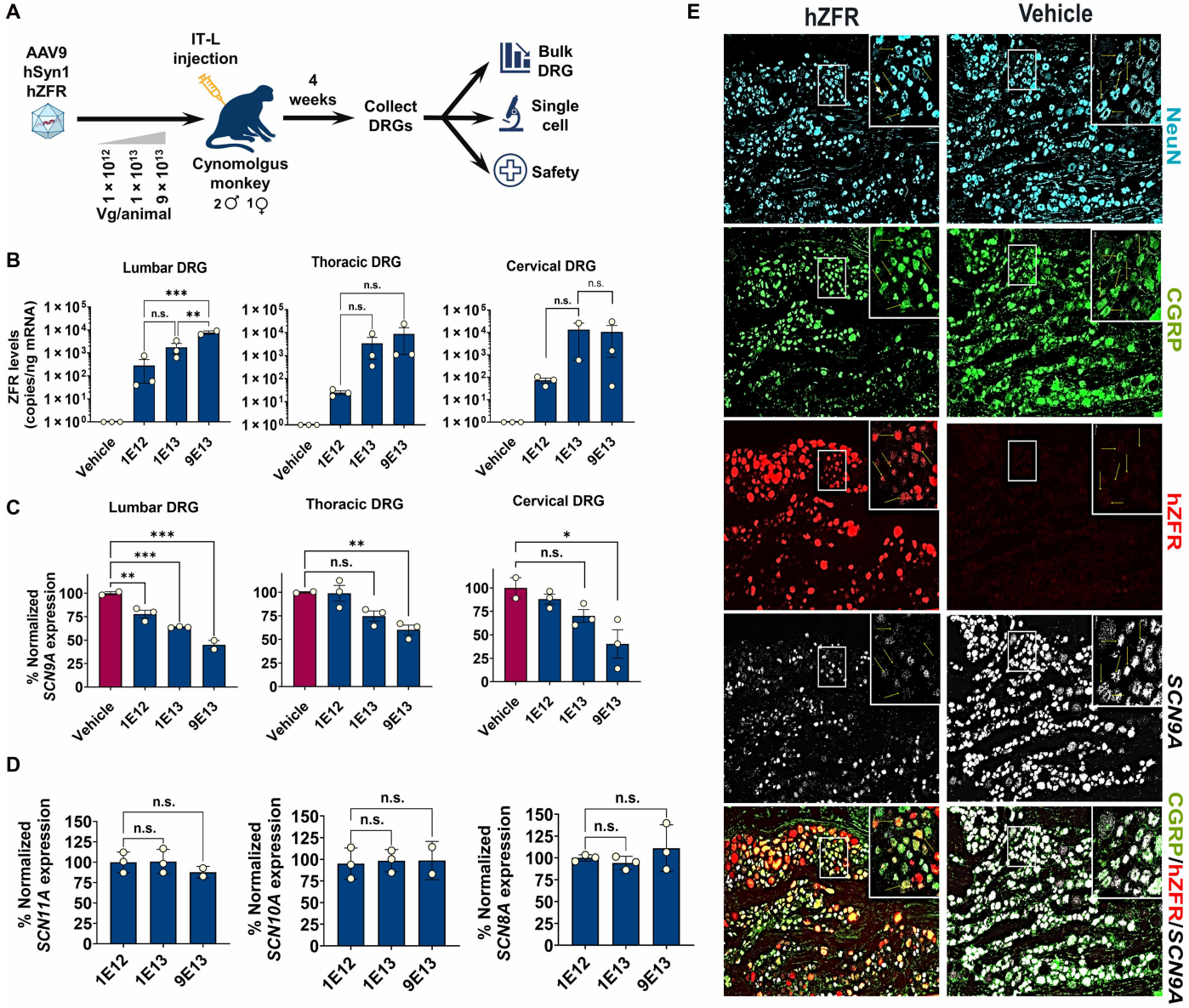

Fig. 4. Dose-dependent repression of *SCN9A* in multiple DRG levels 1 month after IT-L injection in NHPs. (**A**) Overview and timeline of the NHP study evaluating the potency and safety of the hZFR. (**B**) Average AAV9-hZFR expression in NHP lumbar, thoracic, and cervical DRGs, 4 weeks after IT-L injection at three different doses. Dots represent an individual NHP. Means ± SEM. (**C**) Normalized average mRNA expression of *SCN9A* in NHP lumbar, thoracic, and cervical DRGs. *SCN9A* levels were reduced by 40 to 60% at the bulk DRG tissue level across a 100-fold dose range 4 weeks postinjection. Dots represent an individual NHP. Means ± SEM; one-way ANOVA, $^{**}P < 0.01$; $^{***}P < 0.001$; $^{****}P < 0.0001$ compared with the vehicle group. (**D**) Normalized average mRNA expression of SCN8A (Nav1.6), SNC10A (Nav1.8), and SCN11A (Nav1.9) in lumbar DRGs after ZFR treatment. Means ± SEM; one-way ANOVA, $^{**}P < 0.01$; $^{***}P < 0.001$; $^{****}P < 0.0001$ compared with the vehicle group. (**E**) Representative images illustrating the reduction of *Scn9a* mRNA in AAV9-hZFR–expressing nociceptors. The left column shows lumbar DRG sections obtained from the hZFR-treated NHPs, and the right column shows sections obtained from the vehicle-treated NHPs. Lumbar DRG sections from NHPs injected with the high dose (9×10^{13} vg per animal) of AAV9-hZFR or vehicle control were immunolabeled for NeuN [neuronal marker (teal)] and CGRP [nociceptive marker (green)] and hybridized with a fluorescently labeled NHP-specific *SCN9A* RNA probe (white) and ZFR RNA probe (red). Scale bars, 50 μm.

RNAscope evaluated the ZFR-mediated repression of *SCN9A* on a single-cell level. Unlike mice, the cellular and molecular bases of nociception in NHPs are less understood, and much less is known about characteristics of neuronal populations in NHPs or human DRGs. We tested several commercially available antibodies against proteins predicted to be expressed in nociceptors in higher species such as calcitonin gene-related peptide (CGRP; CALCA), isolectin B4 (IB4; P2X3R), and tachykinin precursor 1 (TAC1; substance P). Among all tested antibodies, an antibody against CGRP demonstrated a consistent and distinct signal and was thus selected to further characterize the expression of *SCN9A* in nociceptors in NHP lumbar DRGs. It has been shown before that ~60% of CGRP+ neurons in human DRGs are positive for *SCN9A* (*29*). An antibody against NeuN (neuronal marker) was used to assess the total neuronal population in the DRGs. These antibodies were combined with RNAscope to assess *SCN9A* mRNA in nociceptors after hZFR injection (Fig. 4E). *SCN9A* mRNA (white) was observed throughout lumbar DRGs in CGRP+ cells (green) in vehicle-treated NHPs. A reduction of the *SCN9A* mRNA transcript was observed in CGRP+ cells that were also hZFR+ (Fig. 4E), illustrating that ZFRs can reduce expression of the *SCN9A* transcript in NHP DRG nociceptors. Together, the 1-month study demonstrated the potency and specificity of hZFR in NHP DRGs.

Dose-limiting toxicity was not observed after AAV9-mediated delivery of hZFR in the 1-month DRF

hZFR was well tolerated in cynomolgus monkeys, with all animals surviving for the duration of the 1-month study. There were no AAV9-hZFR–related abnormal clinical signs or changes in behavior. We evaluated the standard clinical chemistry, hematology, and coagulations panels, and no findings related to hZFR administration were observed, including no changes in liver enzymes [alanine transaminase (ALT), aspartate aminotransferase (AST), or total bilirubin (TBIL)] (Fig. 5A) or hematology assessments [white blood cells (WBC), leukocytes, or neutrophils] (Fig. 5B), coagulation [platelet count (PLT), prothrombin time (PT), or fibrinogen (FIB)] (Fig. 5C), metabolic [cholesterol, low-density lipoprotein (LDL), or glucose] (Fig. 5D), or kidney function [creatinine, blood urea nitrogen (BUN), and lactate dehydrogenase (LDH)] (Fig. 5E) parameters.

Histopathology assessment was performed for the following tissues: adrenal glands, brain, DRGs (sacral, lumbar, thoracic, and cervical), epididymis, heart, kidney, small and large intestines, liver, lung, lymph node (mandibular), ovary, pancreas, sciatic nerve, skeletal muscle, spinal cord (lumbar, thoracic, and cervical), spleen, stomach, testes, thymus, trigeminal ganglia, and uterus/cervix. Microscopic analysis showed no treatment-related findings in the brain or other collected tissues, except for DRGs, trigeminal ganglia, and

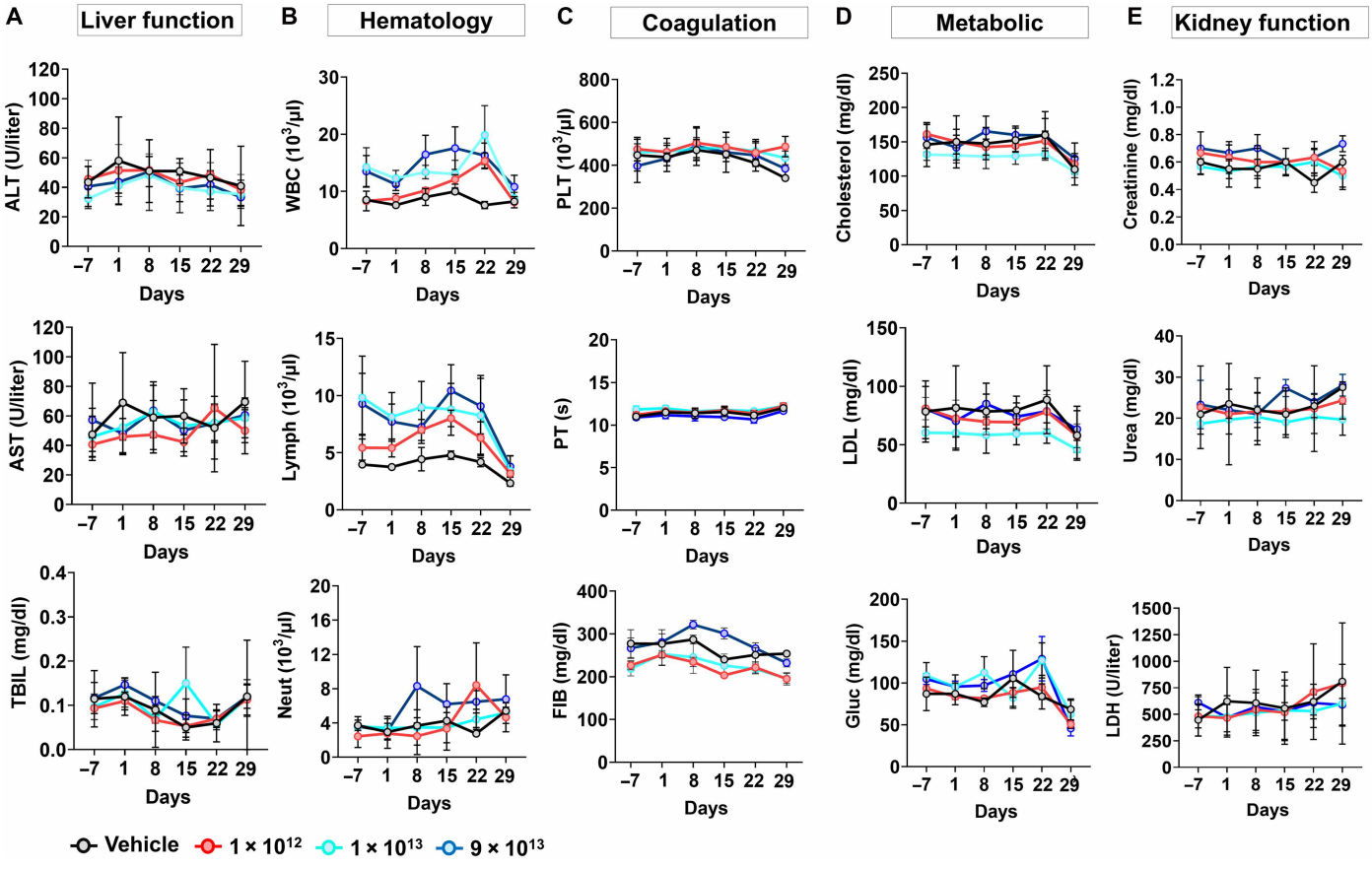

Fig. 5. AAV9-hZFR treatment does not induce any changes in markers of clinical pathology. (**A** to **E**) Various blood markers for different physiological functions were evaluated 7 days before injection (−7) and at different time points after AAV9-hZFR IT injection (days 1, 8, 15, 22, and 29) for all three dose groups and vehicle-treated animals ($N = 4$ per group). Markers for liver function (ALT, AST, and TBIL) (A), hematology [WBCs, lymphocytes (Lymph), and neutrophils (Neut)] (B), coagulation (PLT, PT, and FIB) (C), metabolic function [cholesterol, LDL, and glucose (Gluc)] (D), and kidney function (creatinine, urea, and LDH) (E). Means ± SEM.

spinal cords. Predominantly dose-dependent microscopic findings were observed at doses ≥ 1×10^{12} vg per animal in the trigeminal ganglia and DRGs of minimal degeneration/necrosis of single neurons and spinal cord including minimal axonal degeneration of the dorsal funiculus and minimal mononuclear cell infiltrates of the lumbar dorsal roots (Fig. 6 and fig. S6). These minimal to mild findings are known class effects of AAV gene therapies in NHPs (*30*–*33*) and thought to be primarily related to overexpression of transgenes in neurons and associated effects on axons originating from these neurons (*34*, *35*).

Persistent repression of *SCN9A* in DRGs does not lead to dose-limiting toxicity 6 months after IT-L delivery of the clinical product ST-503

The pharmacology and safety profile of AAV9-hZFR in NHPs supported early development of the ST-503, an investigational product

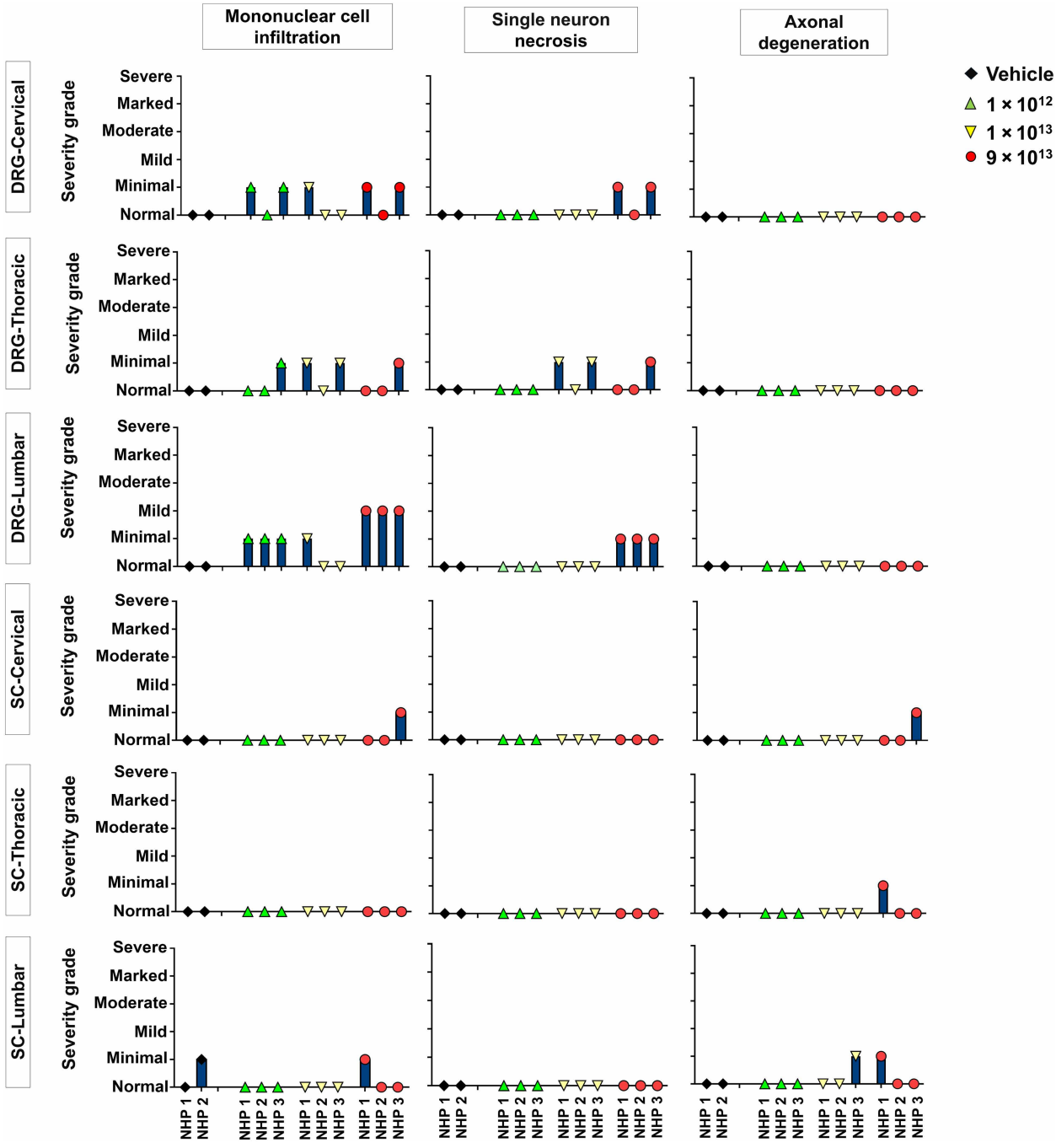

Fig. 6. Minimal to mild microscopic findings in DRGs and spinal cords in NHPs 1 month after AAV9-hZFR administration. The profiles of histopathological findings in DRGs and spinal cord are illustrated for each individual animal in the 1-month NHP dose range-finding study. Each symbol represents an individual animal in the respective dose group.

for the treatment of patients with neuropathic pain. ST-503 contains a similar vector construct to AAV9-hZFR, also using the neuron-specific Syn1 promoter. Pharmacology and safety of ST-503 were evaluated in cynomolgus monkeys in a Good Laboratory Practice (GLP) 6-month pharmacology and toxicology study after a single one-time IT-L administration at 9×10^{13} vg per animal (Fig. 7A). At 6 months postdosing, assessment of bulk DRG tissues (lumbar, thoracic, and cervical) showed the expression of ST-503 in all three DRG levels (Fig. 7B). One animal showed lower expression levels (red circle), and that translated to lower repression of *SCN9A* in that animal's DRGs (Fig. 7C, red circle). About 50% repression of *SCN9A* in all three DRG levels was observed for other animals, illustrating persistent repression of *SCN9A* in NHPs up to 6 months (Fig. 7C). ST-503 was well tolerated, with all animals surviving until

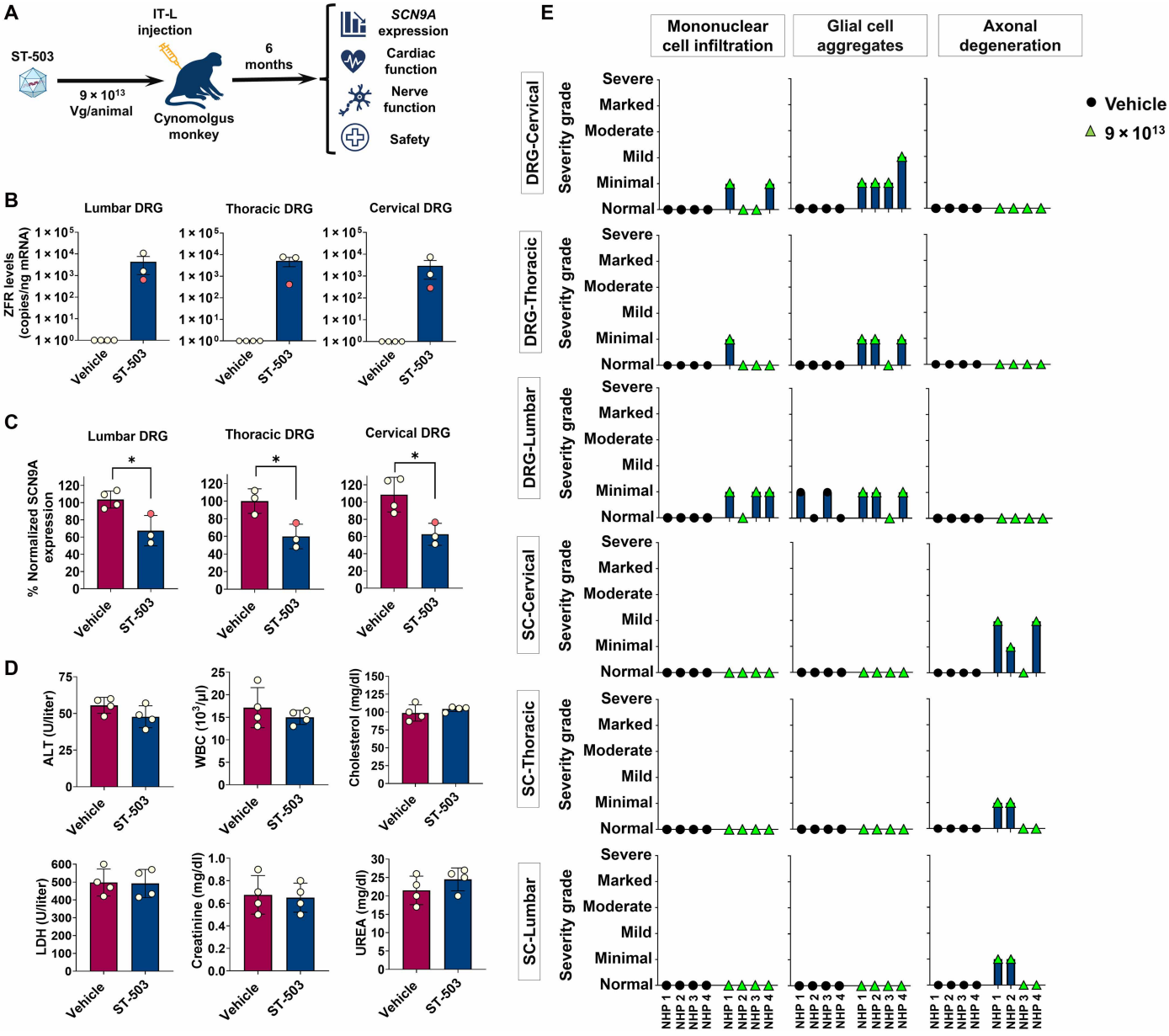

Fig. 7. ST-503 IT-L administration leads to durable repression of *SCN9A* with AAV class–related microscopic findings in the DRGs 6 months after treatment. (**A**) Overview of the 6-month NHP study with ST-503 evaluating pharmacology and safety. (**B**) Average ST-503 expression in NHP lumbar, thoracic, and cervical DRGs, 6 months after IT-L injection. Circles represent an individual NHP. Red circle represents an animal that was not properly dosed, $n = 4$. Total RNA was not sufficiently isolated from one animal in the ST-503 group. (**C**) Normalized mRNA expression of *SCN9A* in NHP lumbar, thoracic, and cervical DRGs 6 months after ST-503 treatment. Dots represent an individual NHP. Means ± SEM; *t* test, $^{**}P < 0.01$; $^{***}P < 0.001$; $^{****}P < 0.0001$ compared with the vehicle group, $N = 4$. Total RNA was not sufficiently isolated from one animal in the ST-503 group and not included on the graph. (**D**) Various clinical chemistry and hematology parameters were evaluated 6 months after ST-503 administration at 9×10^{13} vg per animal and vehicle-treated animals. Means ± SEM. (**E**) The severity profiles of histopathological findings in DRGs (cervical, thoracic, and lumbar) and spinal cords (cervical, thoracic, and lumbar) are illustrated for each individual animal in the 6-month NHP study. The estimate severity was based on % tissue damage: <10%: minimal; 10 to 30%: mild; 30 to 60%: moderate; 60 to 99%: marked; >99%: severe.

scheduled necropsy. There were no ST-503–related adverse findings in clinical pathology, hematology, or coagulation assessments (Fig. 7D). The same list of tissues evaluated in the 1-month NHP study were evaluated in the 6-month study. ST-503–related microscopic findings observed at 6 months in the DRGs, dorsal funiculi of the spinal cord, trigeminal ganglia, and lumbar dorsal nerve roots were of minimal to rarely mild severity. The DRGs and trigeminal ganglia had minimal neuronal degeneration, minimal to mild mononuclear cell infiltration, and minimal to mild glial cell aggregates. The dorsal funiculi of the spinal cord and cervical dorsal nerve roots had minimal to mild axonal degeneration with minimal increased Schwann cells in cervical dorsal nerve roots (Fig. 7E). No microscopic findings were observed in sciatic or median nerves (fig. S7) or other tissues.

ST-503 administration shows no treatment-related adverse effects on neurologic evaluations, qualitative and quantitative ECG, heart rate, blood pressure, or nerve conduction velocity assessments 6 months postdose

Neurological evaluations included evaluation of general attitude, behavior, motor function, cranial nerves, proprioception and postural reactions, and spinal nerves (fig. S8). All ST-503–administered animals were observed under normal conditions compared with the vehicle group and relative to the start date. Nerve conduction velocity studies were performed to evaluate possible adverse effects after ST-503 administration. There were no changes in peroneal motor, sural sensory, or median sensory nerve conduction velocity or amplitude for up to 6 months compared to vehicle-treated animals. Similarly, there were no changes noted in the onset latency of the cauda equina up to 6 months postdosing (Fig. 8A). There were no ST-503–related findings in qualitative and quantitative electrocardiogram (ECG) evaluations, heart rate, blood pressure (systolic or diastolic), and arterial pressure assessments 6 months after a single IT-L administration at 9×10^{13} vg per animal (Fig. 8B). These results demonstrate that nerve and sensory functions are unaffected up to 6 months after ST-503 administration, similar to what has been reported in the literature after AAV gene therapy administered to the central nervous system or systemically (*35*, *36*).

DISCUSSION

Peripheral neuropathy represents a major health burden and a globally unmet clinical need (*36*), and this type of pain is associated with greater anxiety, depression, and sleep disturbance than nonneuropathic pain (*37*). Current medications indicated for treatment of neuropathic pain may potentially provide some relief, but the effect sizes for these drugs are small, and treatments are often associated with serious adverse effects. Moreover, many patients will not obtain sufficient pain relief at tolerated doses (*1*, *37*–*40*). Opioids are another treatment option for neuropathic pain yet can be accompanied by a range of harmful secondary side effects and addictive potential (*41*). Considering the lack of long-lasting and safe treatments for chronic neuropathic pain, there is an urgent need for new drugs for chronic pain management, and genomic medicines may offer an attractive alternative approach for neuropathic pain.

Nav1.7 has gained much attention in the past couple of decades because of findings that loss or gain-of-function mutations in *SCN9A* lead to loss of or excessive pain sensation in patients, respectively, providing genetic evidence for the Nav1.7 sodium channel as a therapeutic target for pain (*14*, *15*, *42*). Most attempts to develop specific small-molecule inhibitors targeting Nav1.7, however, have failed in the clinic. Several reasons have been proposed for failures, such as insufficient Nav1.7 channel blockade (*18*, *43*). One of the key issues has been a lack of selectivity toward the Nav1.7 channel, resulting in adverse effects associated with inadvertently targeting other Nav channels (*44*–*47*) in the peripheral and central nervous systems. Nav channels share many sequence and structural similarities and play

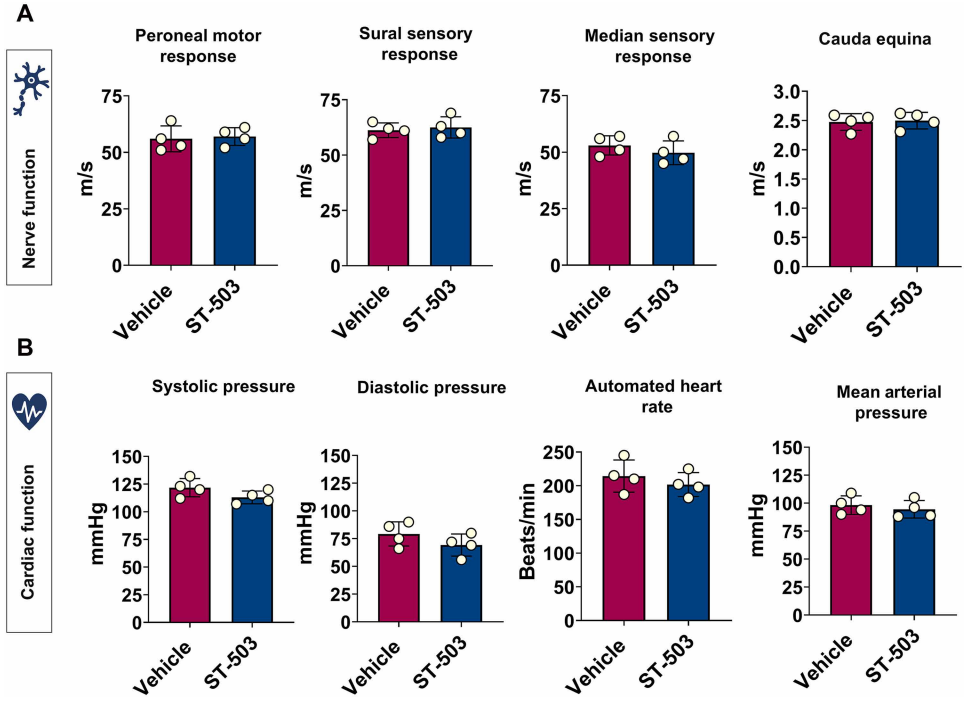

Fig. 8. ST-503 does not induce changes in nerve conduction velocity, heart rate, or blood pressure at 6 months after IT-L injection in NHPs. (**A**) Nerve conduction velocity assessments were performed 6 months after ST-503 administration at 9×10^{13} vg per animal. Peroneal motor nerve responses, sural sensory nerve responses, median sensory nerve responses, and the cauda equina responses were measured for vehicle- or ST-503–dosed animals. (**B**) Cardiac function was evaluated by measuring the blood pressure and heart rate 6 months after ST-503 administration. Dots represent individual animals. Means ± SEM.

critical roles in maintaining neuronal excitability in different tissues. Thus, inadvertently targeting these sodium channels may have unwanted clinical consequences. Nav1.1, Nav1.2, and Nav1.3 are mainly expressed in the brain, and loss of function in these channels is linked to epilepsy and autism. Nav1.4 and Nav1.5 are expressed predominantly in the muscular and cardiovascular systems and are responsible for maintaining muscle and cardiac cell action potentials (*8*). Nav1.6, Nav1.8, and Nav1.9 are mainly expressed in the DRGs and, like Nav1.7, have been implicated in pain pathways (*48*). Recently, a selective small-molecule inhibitor targeting Nav1.8 has shown promising results in clinical trials for acute pain (*17*). However, genome-wide association studies (GWASs) and other analyses revealed that loss of function mutations in Nav1.8 may lead to Brugada syndrome (sudden death syndrome) and cardiac arrest (*49*–*51*); thus, the long-term effect and safety of Nav1.8 inhibitors in the clinic remain to be established.

Considering the wide expression and range of functions Nav channels play in the body, it is critical to develop a selective repressor for Nav1.7 for repression of neuropathic pain. Using the specificity of ZFRs in targeting precise DNA sequences, we have identified distinct sequences and binding sites near the human/NHP *SCN9A* TSS that are not shared with other Nav channels. Global transcriptomic analysis revealed that hZFR only represses the expression of *SCN9A*, and no other genes are differentially regulated including other Nav channels in human iPSC-derived GABAergic and sensory neurons (Fig. 1). In correlation, no changes in the gene expression of Nav1.6, Nav1.8, or Nav1.9 were observed in NHP bulk DRG tissue analysis 1 month after IT-L treatment with hZFR (Fig. 4). Collectively, these data demonstrate that hZFR or other human ZFRs with similar sequences as hZFR selectively and specifically target *SCN9A* in vitro and in mice and NHPs in vivo.

IT-L administration of hZFR and the clinical investigational product ST-503 to cynomolgus monkeys demonstrated ZFR mRNA expression capable of reducing bulk *SCN9A* mRNA expression to similar levels as seen in the SNI neuropathic pain model in mice administered mZFRs, suggesting that delivery, expression, and activity of ZFRs in NHPs may translate to patients and provide therapeutic benefit. Similar data were obtained at the single-cell level in NHP lumbar DRG neurons, exhibiting repression of *SCN9A* in ZFR+ nociceptors, further demonstrating potency of ZFRs and that low cellular levels of ZFRs are effective at reducing up to 90% of target *SCN9A* expression in a single cell. The degree of inhibition of *SCN9A* needed to effectively reverse neuropathic pain in the clinic has not yet been established. Individuals, however, who are heterozygous for a loss-of-function mutation of Nav1.7 (individuals who have only one functional allele of *SCN9A* and presumably express 50% of functional Nav1.7 protein) exhibit normal pain responses (*15*), indicating that 50% repression of Nav1.7 should be sufficient to establish a normal pain response. In the SNI neuropathic pain mouse model, we showed that 60% repression of *Scn9a* at the bulk DRG level was sufficient to fully restore normal pain responses for mechanical- and cold-induced pain. In addition, hZFR IT-L administration to NHPs showed up to ~60% bulk repression of *SCN9A* in all three DRG levels 1 month postdose, suggesting that hZFR treatment may be sufficient to reduce neuropathic pain in patients. In addition, it should be noted that full repression of Nav1.7 function and pain responses are not desired because complete lack of Nav1.7 expression in humans may lead to a state of insensitivity to pain and the potential for unintended self-injury, such as burning.

The proof-of-concept study in a mouse model of neuropathic pain using surrogate ZFRs targeting mouse *Scn9a* was an important step in preclinical development. This model allows understanding of the relationship among ZFR mRNA expression, *Scn9a* mRNA repression, and efficacy in a pain model. In cynomolgus monkeys, a single IT-L administration of AAV9-hZFR at doses up to 9×10^{13} vg per animal resulted in levels of *SCN9A* repression similar to those observed in our efficacy study and was well tolerated and not associated with ZFR-related adverse effects, including clinical signs, body weights, clinical pathology, and macroscopic observations 1 month after the treatment. Microscopic evaluation associated with AAV9-hZFR treatment showed dose-related but not dose-limiting microscopic findings primarily in the DRGs and the spinal cords, sciatic nerves, and trigeminal ganglia, which has been reported for other AAV gene therapies (*30*–*33*). In the 1-month NHP study, no abnormal behavior indicative of neurological dysfunction or nerve conduction velocity assessments was exhibited by AAV9-hZFR–treated animals.

The proof of concept in the mouse model of neuropathic pain as well as the pharmacology and safety profiles seen in the 1-month NHP DRF study supported identification and development of the ST-503 clinical investigational product for potential treatment of peripheral neuropathy in patients. In the GLP 6-month pharmacology and safety study in NHPs, ST-503 showed persistent repression of *SCN9A*, and administration was not associated with adverse findings in clinical observations, clinical pathology, hematology, coagulation, neurologic, qualitative and quantitative ECG, heart rate, blood pressure, nerve conduction velocity, and macroscopic pathology assessments. ST-503–related microscopic findings at 6 months were limited to minimal to mild mononuclear cell infiltration, minimal neuronal degeneration, and minimal to mild glial cell aggregates in DRGs and trigeminal ganglia; minimal to mild axonal degeneration with minimal increased glial cell aggregates; and minimal to mild axonal degeneration in spinal cords and cervical dorsal nerve roots and minimal increased Schwann cells in cervical dorsal nerve roots. These types of findings are considered AAV class effects.

A meta-analysis of 33 studies with more than 200 NHPs based on published data demonstrated that DRG toxicity is a class effect of AAV gene therapy. Several factors contribute to the incidence and severity of DRG microscopic pathology findings in NHPs, including direct administration into the cerebrospinal fluid (CSF) by intrathecal or intracisternal magna injection and administration of dose levels greater than 1×10^{13} vg per animal (*52*). Incidence and severity are also influenced by route of administration, vector construct design, dose, and animal age (*52*). The meta-analysis revealed that the most severe DRG and spinal cord findings usually occur after the intra-CSF route of administration, with lack of a no observed adverse effect level (NOAEL) established at any dose level above the minimal efficacious dose (1×10^{13} vg per animal) for most transgenes (*52*). The underlying cellular mechanisms that result in degeneration and axonopathy of the DRG sensory nerves after administration of AAV gene therapies have not been fully characterized; however, evidence supports the hypothesis that cellular stress due to high expression of transgene RNA or proteins is involved (*34*, *35*). In addition, the clinical translation of DRG toxicity seen in NHPs is not well understood, with more research needed to understand the mechanisms of toxicity as well as methods to evaluate and mitigate potential sensory neuron toxicity in clinical investigations.

In addition to expression in DRG sensory neurons, several reports have shown that Nav1.7 is also expressed in autonomic afferent C-type

fibers (*53*, *54*), and Nav1.7 inhibition by some small-molecule inhibitors has been shown to cause autonomic deregulation such as hypertension (*33*, *55*). ST-503 administration to NHPs did not lead to a dose-limiting finding 6 months after IT-L administration (Fig. 8). We did not specifically evaluate repression of *SCN9A* in sympathetic ganglia, but the lack of findings in ECG, heart rate, and blood pressure assessments after ST-503 administration are supportive of a low risk of repression of sympathetic neurons (*31*, *32*, *52*, *56*). The expression of AAV9 in sympathetic ganglia has not been studied in NHPs, but in mice, AAV9 intravenous or systemic administration leads to several-fold higher DRG transduction compared with sympathetic neurons in bulk tissue (*57*). Because AAV9 shows high tropism for DRGs and ST-503 ZFR expression is driven by a neuronal-specific promoter, expression of ST-503 may be limited predominantly to neurons in DRGs, which could be an advantage compared with small-molecule inhibitors. No autonomic function abnormalities were reported for PF-05089771, a small-molecule Nav1.7-targeted sodium channel blocker evaluated in individuals with painful diabetic peripheral neuropathy, or vixotrigine, a nonselective voltage-gated sodium channel blocker evaluated for small fiber neuropathy and trigeminal neuralgia (*18, 44*). It is possible that cardiac function abnormalities reported for some small molecules may be related to off-target effects beyond an effect on Nav channels. For example, MK-2075 was developed with selectivity against Nav1.7, but it also showed activity on cardiac ion channels and a broad panel of 114 potential off-targets, which led to cardiac abnormalities such as hypertension (*55*).

Peripheral neuropathies are chronic disorders because neuronal damage is generally not considered reversible given that neurons lack regenerative capacity (*58*). As a result, genomic medicine approaches could potentially provide long-lasting and efficacious treatment for such chronic conditions. The efficacy of genomic medicine targeting *Scn9a* has been illustrated before in preclinical studies. Targeting *Scn9a* RNA with short hairpin RNA (shRNA) or antisense oligonucleotides (ASOs) successfully reduced pain in pain rodent models (*59*, *60*). Targeting RNA, however, is often associated with continuous treatment, off-target toxicity, and insufficient target interactions (*61*), which makes it unsuitable for long-lasting effectiveness for indications such as peripheral neuropathies. AAV-mediated delivery often results in a long-lasting effect in neurons (*62*, *63*), which makes this delivery approach better suited for treatment of chronic peripheral neuropathies. Although AAV9-delivered CRISPR-Cas9 has been used successfully in multiple mouse pain models (*21*), the large size of CRISPR-Cas9 makes it challenging for large-scale production because of insufficient AAV9 packaging. Unlike CRISPR-Cas9, ZFRs are small and compact, allowing for efficient AAV packaging. In addition, ZFRs are human-derived proteins and thus not anticipated to provoke an immune response as anticipated with CRISPR-Cas9 bacterial components, making ZFRs a much more suitable approach for targeting the DRG neurons for potential treatment of peripheral neuropathies.

Our study has some limitations. Pain behavior in NHPs after ZFR treatment was not evaluated because of several restrictions. Pain studies in NHPs are generally prohibited by the institutional animal care committees unless analgesic is administered to alleviate pain, which would have confounded interpretation of results after administration of ST-503. Furthermore, pain assessment in NHPs is challenging because animals tend to conceal signs of discomfort, complicating detection and quantification (*64*). Thus, developing a validated pain assessment protocol would require large number of animals to allow reliable and statistical assessment of pain behavior, which, in NHPs, is prohibitive for ethical reasons. In addition, there are currently no well-accepted NHP models of neuropathic pain, and the in vivo transability and efficacy of hZFR in mice were not measured because of lack of the Nav1.7 humanized mice model. Therefore, translatability of pain reduction from a rodent to a human can only be assessed during clinical trials. Measuring native Nav1.7 protein levels in biological settings has been challenging because of lack of specific antibodies that do not cross-react with other Nav channel proteins, so Nav1.7 protein levels after ZFR treatment were not measured in our studies. As discussed above, minimal to mild DRG toxicity after systemic exposure to AAV gene therapy is a known class effect and has not been dose limiting in clinical studies, including of Zolgensma (an AAV9 product) for the treatment of patients with spinal muscular atrophy. However, from our study, we were unable to directly determine whether the microscopic findings in DRGs were related to a viral vector or gene therapy product. Nevertheless, similar studies have been carried out previously, and neither control AAV nor the cargo had any impact compared to untreated samples or vehicle regarding neuronal function or DRG toxicity (*31*, *35*, *65*).

In conclusion, we have demonstrated that ZFRs targeting human or mouse Nav 1.7 genes can selectively, effectively, and robustly repress expression in vitro and in DRG neurons in mice and cynomolgus monkeys after a single IT-L administration. The proof of concept was demonstrated in a mouse neuropathic pain model, providing insight into ZFR expression and Nav1.7 gene repression in DRG sensory neurons needed for efficacy in pain reduction. ST-503 pharmacology and safety studies in NHPs demonstrated persistent *SCN9A* repression for up to 6 months in DRGs and an acceptable ST-503 safety profile to support future clinical studies in patients with neuropathic pain.

MATERIALS AND METHODS

Study design

Mouse studies were conducted at Afasci (Redwood City, CA, USA) under a protocol approved by the Institutional Animal Care and Use Committee (IACUC). The NHP study was conducted at Charles River Laboratories Inc. (CRL; Reno, NV, USA), which is an Association for Assessment and Accreditation of Laboratory Animal Care International (AAALAC)–accredited facility under an IACUC-approved protocol. IACUC approval at each testing facility for each study are as follows: mice *Scn9a* target engagement study (Fig. 2): NAV_21-11-1; pain assessment in a neuropathic pain mouse model (Fig. 3): 220610NAV1.7SGMO; 1-month pharmacology and safety study in NHPs (Figs. 4 to 6): 20342782; and 6-month pharmacology and safety in NHPs (Figs. 7 and 8): 31998594. All studies were performed in conformance with the US Public Health Policy on the Care and Use of Animals as defined in the Guide to the Care and Use of Animals. Species-specific standard procedures and conditions for animal care, housing, access to water and food, environment, and room maintenance were used. All other procedures were performed in accordance with laboratory standard operating procedures and established laboratory best practices.

Human and mouse ZFR design

DNA sequences encoding chimeric Cys2-His2 zinc finger proteins (ZFPs) coupled with a recognition helix were designed on the basis of a backbone derived from the human ZFP Zif268/EGR1. The recognition

helices were selected from those previously validated for on-target specificity to nucleotide triplets. From this, arrays of five or six fingers (backbone and recognition helices) targeting unique sequences of 15 to 18 nucleotides found near TSSs of the *SCN9A*/*Scn9a* in human (hg38) and mouse (mm10) reference genomes were selected. Sites designed against the human genome were further restricted to regions with homology to *SCN9A* in the cynomolgus monkey (*Macaca fascicularis*; macFas5) reference genome. The target sequences for the mouse and NHP/human ZFRs are presented in table S1. The control AAV-ZFR targets *BC11A* gene and its target sequence are presented in table S1.

Dose range-finding pharmacology and toxicology study in NHPs

This study was conducted at CRL (Reno, NV) under the institutionally approved IACUC (20342782). Naïve, cynomolgus monkeys (sourced from Cambodia) were supplied by CRL and randomly assigned to treatment groups using a computer-based procedure; males and females were randomized separately. Animals were ~3 to 4 years of age at the time of dose administration and weighed 2.1 to 2.4 kg. Randomization also took into account the total antibody (Tab) and neutralizing antibody (Nab) titers against AAV9 to achieve an equal distribution of Tab/Nab+ animals to the extent possible. Female monkeys were housed individually, whereas male monkeys were group housed in accordance with their treatment group. Animal housing included stainless steel cages with mesh floors, and enrichment in the form of socialization, fruit, and cereal was provided. The temperature and humidity in the animal room were 18° to 29°C and 30 to 70%, respectively, with room ventilation being four or more air changes per hour with no air recirculation. The light cycle was 12-hour light and 12-hour dark. Animals received their once daily food ration, and water was provided ad libitum. Monkeys were not immunosuppressed. The study design consists of one vehicle control group ($n = 2$, one male and one female) and three dose groups for hZFR (1×10^{12}, 1×10^{13}, and 9×10^{13} vg per animal; $n = 3$ per group, 2 males and 1 female per group). AAV-hZFR doses were given as a single IT-L injection on day 1, and animals were observed for 28 days postadministration. The volume of administration was 1 ml/NHP. On day 29, animals were placed under deep and unrecoverable anesthesia followed by cardiac perfusion with ice-cold RNase-free phosphate-buffered saline. All tissues collected were preserved in 10% neutral buffered formalin, embedded in paraffin, and processed to blocks.

Microscopic evaluation of tissues from the 1- and 6-month studies in cynomolgus monkeys was conducted by a board-certified veterinary pathologist with experience evaluating US Food and Drug Administration (FDA)–recommended standard panels of tissues collected from cynomolgus monkeys. A detailed microscopic evaluation was performed including all tissues from vehicle control and high-dose groups on selected tissues: spinal cord (cervical, thoracic, and lumbar), sciatic nerve, median nerve, peroneal nerve, sural nerve, DRGs (cervical, thoracic, lumbar, and sacral), and trigeminal ganglion. Spinal cord evaluation included cervical (C2, C4, and C7), thoracic (T2, T4, and T5), and lumbar (L3, L4, and L7) sections, and DRG evaluation included left and right of cervical (C2, C4, and C7), thoracic (T2, T4, and T5), lumbar (L3, L4, and L7), and sacral (S2) segments. The pathologist reviews the entire tissue section on each slide and assigns a severity score when findings are noted for a given tissue type (e.g., DRGs, trigeminal ganglion, nerve or nerve root, and spinal cord). The severity score is based on the % of tissue affected and the number of tissues affected. Grading severities for ST-503–related microscopic findings are listed in table S2. The grading system for histopathological evaluations in tabulated in table S2.

For pharmacology assessment, DRGs were collected from lumbar (L5 and L1), thoracic (T7, T6, and T1), and cervical (C6 and C5) levels and placed in prelabeled tubes and flash frozen in liquid nitrogen. The tubes were kept in a −80°C freezer until analysis.

For single-cell analysis, DRGs were collected and preserved in 10% neutralized buffered formalin at room temperature for 24 hours and then transferred to 70% ethanol and processed to block within 7 days from transfer to ethanol. DRGs were embedded in paraffin and proceed to slides for analysis. Statistical analysis could not be performed for this study due to the limited number of monkeys/ per sex per group.

Study design: 6-month pharmacology and toxicology study in NHPs

This study was conducted at CRL, Reno, NV under the institutional-approved IACUC (31998594). Naïve, cynomolgus monkeys (sourced from Cambodia) were supplied by CRL and randomly assigned to treatment groups using a computer-based procedure; males and females were randomized separately. Animals were ~2.7 to 3.8 years of age at the time of dose administration and weighed 2.0 to 2.8 kg. Procedures for assignment of animals, housing, food, water, light/dark cycle, enrichment, immunosuppression, dosing route and procedure, volume of administration, and method of euthanasia were identical to the 1-month dose range-finding study described earlier. The study design consists of one vehicle control group ($n = 7$, four male and three female) and three dose groups for ST-503 (1×10^{13}, 1×10^{13}, and 9×10^{13} vg per animal; $n = 7$ per group, four males and three female per group). The end points evaluated were identical to the 1-month dose range-finding study with the following exceptions: (i) Nerve conduction velocity and cardiovascular assessment were performed at predose and 1, 3, and 6 months postdose by CRL and evaluated by qualified scientists and veterinary cardiologist and (ii) microscopic pathology was performed on the full tissue list.

ZFR and *SCN9A* mRNA analysis for 1-month dose range-finding and 6-month pharmacology and toxicology studies in NHPs

Each DRG tissue was transferred to 2-ml Eppendorf tubes containing 0.9 ml of TRI Reagent (Thermo Fisher Scientific) and two 3.2-mm steel beads (BioSpec Products) on ice. The tissues were lysed using a Qiagen TissueLyser at 4°C using the following parameters: 15 cycles, 90-s duration, and 25.1 frequency. After centrifugation, 105 μl of 1-bromo-3-chloropropane was added to each sample at room temperature. The samples were vortexed for 10 s, incubated for 5 min at room temperature, and centrifuged at 12,000*g* for 10 min at 4°C. Aqueous phases corresponding to the same original spinal cord level were combined. Four hundred microliters of the aqueous phase from each sample was transferred to a well of a 96 deep-well plate. Two hundred microliters of isopropyl alcohol was added to each sample well containing the aqueous phase of the tissue lysate. Samples were shaken for 1 min at 600 rpm at room temperature. Ten microliters of MagMax magnetic beads (Thermo Fisher Scientific) was added to each sample well and mixed briefly. A KingFisher Flex Purification System (Thermo Fisher Scientific) and a MagMax Total RNA Isolation kit (Thermo Fisher Scientific) were used to isolate RNA from tissue lysates following the manufacturer's instructions. Approximately 100 μl of eluted

RNA was separated from magnetic beads using a magnetic stand by incubating for 5 min at room temperature. Total RNA concentration and quality were evaluated using a Lunatic UV-vis absorbance spectrometer (Unchained Labs). Reverse transcription was prepared using the High-Capacity cDNA Reverse Transcription Kit (Applied Biosystems). Custom TaqMan primer:probe assays and TaqMan 2x Universal PCR Master Mix (Applied Biosystems) were used to perform qPCR using a QuantStudio 6 Flex Real Time PCR Machine (Applied Biosystems). A portion of each reverse transcription reaction was used to carry out two independent qPCR reactions: first for the absolute quantification of ZFR mRNA and second for multiplexed detection of *SCN9A*, *EIF4A2*, and *ATP5B* mRNA. ZFR mRNA copy values were derived from the ZFR standard curve. The obtained ZFR copy values were then divided by the total RNA mass (ng) taken into the qPCR reaction to determine ZFR copies per ng of total RNA. *SCN9A* mRNA fold change was calculated using the 2DeltaDeltaCt method formula where sample DeltaCt was calculated first as a difference between the *SCN9A* cycle threshold (Ct) and the geometric mean of two housekeeping genes Ct and then subtracted by the mean DeltaCt of the assay quality control samples. The *SCN9A* mRNA fold change was then further normalized by dividing the sample fold change values by the mean fold change value from the untreated animals.

Pain assessments in the SNI mouse model

This study was conducted at AfaSci Inc. (Redwood City, CA) under the IACUC no. 220610NAV1.7SGMO. Naïve C57BL/6 female mice (8 per sex per group; ~6 to 10 weeks old) were purchased (from CRL) 1 week before the initiation of the study. Animals were randomly assigned to treatment groups no more than 3 days before dose administration using a manual body weight stratification procedure. Animals from the same treatment group were housed four per cage in polycarbonate, solid-bottom cages containing a nonaromatic bedding and filtered cover. The housing temperature was maintained at 20° to 24°C and humidity was kept at 30 to 70%. Housing rooms had a 12-hour light/12-hour dark cycle with ventilation of at least 10 room volumes/hour with no recirculation of air. Food and water were provided ad libitum. The treatment groups were as follows: sham operated (skin opened and closed but no nerve was cut) to establish that the act of cutting open the skin does not affect pain sensitivity, vehicle control, GBP (50 mg/kg, intraperitoneally given 1 hour before each assessment), or ZFR given IT-L into the L4-L5 or L5-L6 intervertebral space at a single dose of 8×10^{11} vg per mouse. ZFR was formulated in an AAV formulation buffer-P [1X Dulbecco's phosphate-buffered saline (DPBS) (+Ca/+Mg) + 0.001% Pluronic F-68 (pH 7.2)]. Volume of administration was 10 ml per mouse. The dose of GBP was not an anesthetic dose in mice and was selected to reduce but not abolish pain in mice at 0.5 to 1 hour postdose (*66*). The in-life assessments included mortality/morbidity and general health at the cage side daily and detailed clinical observation once weekly. Body weights were measured predose and once weekly. On day 29, mice were euthanized by isoflurane/oxygen anesthesia followed by whole-body transcranial perfusion with RNase-free 0.9% saline. From mice in control- and ZFR-treated groups, three pairs of DRGs were collected from each of the cervical, thoracic, and lumbar regions and transferred to three separate 1.5-ml RNase-free Eppendorf tubes. RNALater was added and tubes were refrigerated (1° to 8°C) for 24 hours. Following 24-hour incubation, tissues were removed from RNALater and transferred to labeled RNase-free Eppendorf tubes. The tubes containing the tissue were then frozen on dry ice and kept in a −80°C freezer until analysis. Dose analysis was performed using RT-qPCR on all dose formulations to assure the accuracy of final dose concentrations.

To generate the model, all animals on day −7 were deeply anesthetized under 2.5% isoflurane in O_2. The left hind leg was shaved and disinfected, and a small incision was made on the skin. The surgical site was opened with blunt dissection to visualize the three distal branches of the sciatic nerve. Two of the three distal branches of the sciatic nerve (tibial and peroneal nerve) were axotomized while sparing one (sural nerve). The surgical site was sutured, and animals were observed for proper wound healing.

Pain assessment (mechanical- and cold-induced) was performed before surgery, 1 week after the surgery, and just before dose administration on day 1 and then on days 3, 8, 15, 22, and 28 postdose. The presurgery measurement was conducted to establish a normal pain baseline for all animals before their assignment to the study. During preassessment, any animal with abnormal pain sensitivity was not used and replaced with another animal to ensure that all animals exhibited a comparable baseline pain level. No animal was excluded from the study based on oversensitivity to pain before surgery or lack of sensitivity to pain 1 week after surgery. Assessment of pain (mechanical- and cold-induced) 7 days postsurgery (just before dose administration) was conducted to assure functionality of the model and to obtain a model baseline as animals that underwent the full surgery should have hypersensitivity to pain.

For the mechanical-induced pain assessment, animals were placed individually into small cages with a mesh bottom. A monofilament (von Frey fibers) was applied perpendicularly to the ventral surface of the left hind paw delivering a constant predetermined force until it buckled, at which time it was removed. A response was considered positive if the animal exhibited any nocifensive behaviors, including brisk paw withdrawal, licking, or shaking of the paw, either during application of the stimulus or immediately after the filament was removed. Testing began with the response to a filament estimated to be close to the 50% withdrawal threshold. If there was no response, the next filament with a higher force was tested; if there was a response, the next lower force filament was tested. Five continuous readings were taken and later assessed to determine withdrawal threshold in grams. For the cold-induced pain assessment, animals were placed on a metal plate after it was cooled to the desired temperature, and the time taken to evoke nociceptive behavior such as flinches, shaking, or licking in the affected paw or jumping was manually scored as paw withdrawal latency in seconds. For SmartCage assessment, animals were placed in the SmartCage system individually and assessed for any movement abnormalities on day 28. Animals were monitored for 22 hours, and data were analyzed at 1-hour blocks.

The technician responsible for pain and SmartCage data collection was blinded to the dose groups. One-way analysis of variance (ANOVA) followed by Dunnett's test was used for body weights, RT-qPCR, and mechanical- and cold-induced pain data. All graphs and statistical analysis used Prism GraphPad. An effect was considered significant if $P < 0.05$.

Mouse and NHP DRG single-cell analysis

For the mouse DRGs, single-cell analysis was performed at Evotech. DRG tissue sections on slides were hybridized with a combination of two RNAscope probes: panZFP probe (ACD Bio, 851651-C2) and MmScn9a probe (ACD Bio, 313341). Following hybridization, sections were stained with an antibody against peripherin (Abcam,

ab246502at) at 1:1000 dilution. 4′,6-Diamidino-2-phenylindole (DAPI) was used in all sections to mark cellular nuclei. The ISH/IHC multiplexing was performed according to the CRO protocol. Images were acquired with an Axio Scan.Z1 slide scanner (Carl Zeiss Microscopy GmbH), using a 20x Plan-apochromat objective (0.8 numerical aperture) and a Hamamatsu Camera. Light-emitting diode (LED) intensity, exposure time, and emission filter settings were kept constant across groups for the acquisition. Images were acquired with a pixel resolution of 0.326 μm by 0.326 μm, inspected in ZEN (v.3.5, Carl Zeiss Microscopy GmbH), and analyzed using custom-written scripts in Acapella Studio 5.1 (PerkinElmer Inc.) before compiling in Spotfire (v.10.3.3 TIBCO).

For the NHP DRGs, the single-cell analysis was performed at ACD Bio. The NHP lumbar DRG was hybridized first with guinea pig anti-NeuN at 1:200 (MilliporeSigma, catalog no. ABN90P) and anti-CGRP (Abcam, catalog no. ab81887). Next, a pooled RNAscope target probe consisting of Mfa-SCN9A (ACD, catalog no. 591588) and pan-ZFP-KRAB-C2 (ACD, catalog no. 851658-C2) was then hybridized for 2 hours at 42°C, followed by a series of amplification steps and rinse steps using RNAscope Multiplex amplification reagents per the manufacturer's instructions (ACD, catalog no. 322800). Last, DAPI was incubated for 10 min at room temperature for nuclear staining. Whole-tissue multiplex imaging was performed at 40X resolution using a 3DHISTECH PANNORAMIC SCAN II digital slide scanner, equipped with SpGr-B, SpOr-B, Cy5.5, and Cy7 filters for visualization of Vivid 520, Vivid 570, Alexa Fluor 647, and Opal 780 fluorophores, respectively.

Statistical analysis

Statistical analysis was performed using GraphPad Prism version 7 (GraphPad Software, San Diego, CA, USA). The statistical test used for each experiment is provided in the associated methods or figure legend. In general, one-way ANOVA with Dunnett's for multiple comparison was used when comparing three or more groups. Significance is indicated by *. The following standard abbreviations are used to reference P values: n.s., not significant; $^{*}P < 0.05$; $^{**}P < 0.01$; $^{***}P < 0.001$; $^{****}P < 0.0001$.

Supplementary Materials

The PDF file includes:
Materials and Methods
Figs. S1 to S8
Tables S1 to S3

Other Supplementary Material for this manuscript includes the following:
Data file S1
MDAR Reproducibility Checklist

REFERENCES AND NOTES

1. N. Attal, M. Lanteri-Minet, B. Laurent, J. Fermanian, D. Bouhassira, The specific disease burden of neuropathic pain: Results of a French nationwide survey. *Pain* **152**, 2836–2843 (2011).
2. N. Torrance, B. H. Smith, M. I. Bennett, A. J. Lee, The epidemiology of chronic pain of predominantly neuropathic origin. Results from a general population survey. *J. Pain* **7**, 281–289 (2006).
3. T. S. Jensen, R. Baron, M. Haanpää, E. Kalso, J. D. Loeser, A. S. C. Rice, R. D. Treede, A new definition of neuropathic pain. *Pain* **152**, 2204–2205 (2011).
4. A. B. O'Connor, Neuropathic pain: Quality-of-life impact, costs and cost effectiveness of therapy. *Pharmacoeconomics* **27**, 95–112 (2009).
5. B. Bingham, S. K. Ajit, D. R. Blake, T. A. Samad, The molecular basis of pain and its clinical implications in rheumatology. *Nat. Clin. Pract. Rheumatol.* **5**, 28–37 (2009).
6. R. S. Y. Ma, K. Kayani, D. W. Oshodi, A. Whyte Oshodi, N. Nachiappan, S. Gnanarajah, R. Mohammed, Voltage gated sodium channels as therapeutic targets for chronic pain. *J. Pain Res.* **12**, 2709–2722 (2019).
7. M. de Lera Ruiz, R. L. Kraus, Voltage-gated sodium channels: Structure, function, pharmacology, and clinical indications. *J. Med. Chem.* **58**, 7093–7118 (2015).
8. F. H. Yu, W. A. Catterall, Overview of the voltage-gated sodium channel family. *Genome Biol.* **4**, 207 (2003).
9. J. P. Drenth, S. G. Waxman, Mutations in sodium-channel gene SCN9A cause a spectrum of human genetic pain disorders. *J. Clin. Invest.* **117**, 3603–3609 (2007).
10. T. R. Cummins, S. D. Dib-Hajj, S. G. Waxman, Electrophysiological properties of mutant Nav1.7 sodium channels in a painful inherited neuropathy. *J. Neurosci.* **24**, 8232–8236 (2004).
11. Y. Yang, Y. Wang, S. Li, Z. Xu, H. Li, L. Ma, J. Fan, D. Bu, B. Liu, Z. Fan, G. Wu, J. Jin, B. Ding, X. Zhu, Y. Shen, Mutations in SCN9A, encoding a sodium channel alpha subunit, in patients with primary erythermalgia. *J. Med. Genet.* **41**, 171–174 (2004).
12. C. R. Fertleman, M. D. Baker, K. A. Parker, S. Moffatt, F. V. Elmslie, B. Abrahamsen, J. Ostman, N. Klugbauer, J. N. Wood, R. M. Gardiner, M. Rees, SCN9A mutations in paroxysmal extreme pain disorder: Allelic variants underlie distinct channel defects and phenotypes. *Neuron* **52**, 767–774 (2006).
13. J. J. Cox, F. Reimann, A. K. Nicholas, G. Thornton, E. Roberts, K. Springell, G. Karbani, H. Jafri, J. Mannan, Y. Raashid, L. Al-Gazali, H. Hamamy, E. M. Valente, S. Gorman, R. Williams, D. P. McHale, J. N. Wood, F. M. Gribble, C. G. Woods, An SCN9A channelopathy causes congenital inability to experience pain. *Nature* **444**, 894–898 (2006).
14. S. D. Dib-Hajj, T. R. Cummins, J. A. Black, S. G. Waxman, From genes to pain: $Na_v1.7$ and human pain disorders. *Trends Neurosci.* **30**, 555–563 (2007).
15. S. D. Dib-Hajj, Y. Yang, J. A. Black, S. G. Waxman, The $Na_V1.7$ sodium channel: From molecule to man. *Nat. Rev. Neurosci.* **14**, 49–62 (2013).
16. L. A. McDermott, G. A. Weir, A. C. Themistocleous, A. R. Segerdahl, I. Blesneac, G. Baskozos, A. J. Clark, V. Millar, L. J. Peck, D. Ebner, I. Tracey, J. Serra, D. L. Bennett, Defining the functional role of $Na_V1.7$ in human nociception. *Neuron* **101**, 905–919.e8 (2019).
17. S. Ahmad, L. Dahllund, A. B. Eriksson, D. Hellgren, U. Karlsson, P. E. Lund, I. A. Meijer, L. Meury, T. Mills, A. Moody, A. Morinville, J. Morten, D. O'Donnell, C. Raynoschek, H. Salter, G. A. Rouleau, J. J. Krupp, A stop codon mutation in SCN9A causes lack of pain sensation. *Hum. Mol. Genet.* **16**, 2114–2121 (2007).
18. A. McDonnell, S. Collins, Z. Ali, L. Iavarone, R. Surujbally, S. Kirby, R. P. Butt, Efficacy of the $Na_V1.7$ blocker PF-05089771 in a randomised, placebo-controlled, double-blind clinical study in subjects with painful diabetic peripheral neuropathy. *Pain* **159**, 1465–1476 (2018).
19. M. E. Rothenberg, M. Tagen, J. H. Chang, J. Boyce-Rustay, M. Friesenhahn, D. H. Hackos, A. Hains, D. Sutherlin, M. Ward, W. Cho, Correction to: Safety, tolerability, and pharmacokinetics of GDC-0276, a novel $Na_V1.7$ inhibitor, in a first-in-human, single- and multiple-dose study in healthy volunteers. *Clin. Drug Investig.* **39**, 889–890 (2019).
20. M. Imbeault, P. Y. Helleboid, D. Trono, KRAB zinc-finger proteins contribute to the evolution of gene regulatory networks. *Nature* **543**, 550–554 (2017).
21. A. M. Moreno, F. Alemán, G. F. Catroli, M. Hunt, M. Hu, A. Dailamy, A. Pla, S. A. Woller, N. Palmer, U. Parekh, D. McDonald, A. J. Roberts, V. Goodwill, I. Dryden, R. F. Hevner, L. Delay, G. Gonçalves dos Santos, T. L. Yaksh, P. Mali, Long-lasting analgesia via targeted in situ repression of $Na_V1.7$ in mice. *Sci. Transl. Med.* **13**, eaay9056 (2021).
22. B. Zeitler, S. Froelich, K. Marlen, D. A. Shivak, Q. Yu, D. Li, J. R. Pearl, J. C. Miller, L. Zhang, D. E. Paschon, S. J. Hinkley, I. Ankoudinova, S. Lam, D. Guschin, L. Kopan, J. M. Cherone, H. O. B. Nguyen, G. Qiao, Y. Ataei, M. C. Mendel, R. Amora, R. Surosky, J. Laganiere, B. J. Vu, A. Narayanan, Y. Sedaghat, K. Tillack, C. Thiede, A. Gärtner, S. Kwak, J. Bard, L. Mrzljak, L. Park, T. Heikkinen, K. K. Lehtimäki, M. M. Svedberg, J. Häggkvist, L. Tari, M. Tóth, A. Varrone, C. Halldin, A. E. Kudwa, S. Ramboz, M. Day, J. Kondapalli, D. J. Surmeier, F. D. Urnov, P. D. Gregory, E. J. Rebar, I. Muñoz-Sanjuán, H. S. Zhang, Allele-selective transcriptional repression of mutant HTT for the treatment of Huntington's disease. *Nat. Med.* **25**, 1131–1142 (2019).
23. S. Wegmann, S. L. DeVos, B. Zeitler, K. Marlen, R. E. Bennett, M. Perez-Rando, D. MacKenzie, Q. Yu, C. Commins, R. N. Bannon, B. T. Corjuc, A. Chase, L. Diez, H. O. B. Nguyen, S. Hinkley, L. Zhang, A. Goodwin, A. Ledeboer, S. Lam, I. Ankoudinova, H. Tran, N. Scarlott, R. Amora, R. Surosky, J. C. Miller, A. B. Robbins, E. J. Rebar, F. D. Urnov, M. C. Holmes, A. M. Pooler, B. Riley, H. S. Zhang, B. T. Hyman, Persistent repression of tau in the brain using engineered zinc finger protein transcription factors. *Sci. Adv.* **7**, eabe1611 (2021).
24. Y. E. Tak, G. Boulay, L. Lee, S. Iyer, N. T. Perry, H. T. Schultz, S. P. Garcia, L. Broye, J. E. Horng, S. Rengarajan, B. Naigles, A. Volorio, J. D. Sander, J. Gong, N. Riggi, J. K. Joung, M. N. Rivera, Genome-wide functional perturbation of human microsatellite repeats using engineered zinc finger transcription factors. *Cell Genom.* **2**, 100119 (2022).
25. J. F. Margolin, J. R. Friedman, W. K. Meyer, H. Vissing, H. J. Thiesen, F. J. Rauscher III, Kruppel-associated boxes are potent transcriptional repression domains. *Proc. Natl. Acad. Sci. U.S.A.* **91**, 4509–4513 (1994).
26. B. L. Ellis, M. L. Hirsch, J. C. Barker, J. P. Connelly, R. J. Steininger III, M. H. Porteus, A survey of ex vivo/in vitro transduction efficiency of mammalian primary cells and cell lines with

Nine natural adeno-associated virus (AAV1-9) and one engineered adeno-associated virus serotype. *Virol. J.* **10**, 74 (2013).
27. L. Cao, A. M. Donnell, A. Nitzsche, A. Alexandrou, P.-P. Saintot, A. J. C. Loucif, A. R. Brown, G. Young, M. Mis, A. Randall, S. G. Waxman, P. Stanley, S. Kirby, S. Tarabar, A. Gutteridge, R. Butt, R. M. McKernan, P. Whiting, Z. Ali, J. Bilsland, E. B. Stevens, Pharmacological reversal of a pain phenotype in iPSC-derived sensory neurons and patients with inherited erythromelalgia. *Sci. Transl. Med.* **8**, 335ra356 (2016).
28. M. Richner, O. J. Bjerrum, A. Nykjaer, C. B. Vaegter, The spared nerve injury (SNI) model of induced mechanical allodynia in mice. *J. Vis. Exp.* , 3092 (2011).
29. S. Shiers, R. M. Klein, T. J. Price, Quantitative differences in neuronal subpopulations between mouse and human dorsal root ganglia demonstrated with RNAscope in situ hybridization. *Pain* **161**, 2410–2424 (2020).
30. C. Hinderer, N. Katz, E. L. Buza, C. Dyer, T. Goode, P. Bell, L. K. Richman, J. M. Wilson, Severe toxicity in nonhuman primates and piglets following high-dose intravenous administration of an adeno-associated virus vector expressing human SMN. *Hum. Gene Ther.* **29**, 285–298 (2018).
31. J. Hordeaux, C. Hinderer, T. Goode, E. L. Buza, P. Bell, R. Calcedo, L. K. Richman, J. M. Wilson, Toxicology study of intra-cisterna magna adeno-associated virus 9 expressing iduronate-2-sulfatase in rhesus macaques. *Mol. Ther. Methods Clin. Dev.* **10**, 68–78 (2018).
32. J. Hordeaux, C. Hinderer, T. Goode, N. Katz, E. L. Buza, P. Bell, R. Calcedo, L. K. Richman, J. M. Wilson, Toxicology study of intra-cisterna magna adeno-associated virus 9 expressing human alpha-L-iduronidase in rhesus macaques. *Mol. Ther. Methods Clin. Dev.* **10**, 79–88 (2018).
33. J. B. Rosenberg, A. Chen, B. P. de, J. P. Dyke, D. J. Ballon, S. Monette, R. J. Ricart Arbona, S. M. Kaminsky, R. G. Crystal, D. Sondhi, Safety of direct intraparenchymal AAVrh.10-mediated central nervous system gene therapy for metachromatic leukodystrophy. *Hum. Gene Ther.* **32**, 563–580 (2021).
34. N. Buss, L. Lanigan, J. Zeller, D. Cissell, M. Metea, E. Adams, M. Higgins, K. H. Kim, E. Budzynski, L. Yang, Y. Liu, M. Butt, O. Danos, M. Fiscella, Characterization of AAV-mediated dorsal root ganglionopathy. *Mol. Ther. Methods Clin. Dev.* **24**, 342–354 (2022).
35. J. Hordeaux, E. L. Buza, B. Jeffrey, C. Song, T. Jahan, Y. Yuan, Y. Zhu, P. Bell, M. Li, J. A. Chichester, R. Calcedo, J. M. Wilson, MicroRNA-mediated inhibition of transgene expression reduces dorsal root ganglion toxicity by AAV vectors in primates. *Sci. Transl. Med.* **12**, eaba9188 (2020).
36. A. H. Doth, P. T. Hansson, M. P. Jensen, R. S. Taylor, The burden of neuropathic pain: A systematic review and meta-analysis of health utilities. *Pain* **149**, 338–344 (2010).
37. L. Colloca, T. Ludman, D. Bouhassira, R. Baron, A. H. Dickenson, D. Yarnitsky, R. Freeman, A. Truini, N. Attal, N. B. Finnerup, C. Eccleston, E. Kalso, D. L. Bennett, R. H. Dworkin, S. N. Raja, Neuropathic pain. *Nat. Rev. Dis. Primers* **3**, 17002 (2017).
38. N. Attal, Pharmacological treatments of neuropathic pain: The latest recommendations. *Rev. Neurol. (Paris)* **175**, 46–50 (2019).
39. N. B. Finnerup, N. Attal, S. Haroutounian, E. McNicol, R. Baron, R. H. Dworkin, I. Gilron, M. Haanpää, P. Hansson, T. S. Jensen, P. R. Kamerman, K. Lund, A. Moore, S. N. Raja, A. S. C. Rice, M. Rowbotham, E. Sena, P. Siddall, B. H. Smith, M. Wallace, Pharmacotherapy for neuropathic pain in adults: A systematic review and meta-analysis. *Lancet Neurol.* **14**, 162–173 (2015).
40. N. Nishikawa, M. Nomoto, Management of neuropathic pain. *J. Gen. Fam. Med.* **18**, 56–60 (2017).
41. E. D. McNicol, A. Midbari, E. Eisenberg, Opioids for neuropathic pain. *Cochrane Database Syst. Rev.* **2013**, CD006146 (2013).
42. S. G. Waxman, S. D. Dib-Hajj, $Na_V1.7$: A central role in pain. *Neuron* **111**, 2615–2617 (2023).
43. C. G. Faber, N. Attal, G. Lauria, R. H. Dworkin, R. Freeman, K. T. Dawson, H. Finnigan, A. Hajihosseini, H. Naik, M. Serenko, C. J. Morris, M. Kotecha, Efficacy and safety of vixotrigine in idiopathic or diabetes-associated painful small fibre neuropathy (CONVEY): A phase 2 placebo-controlled enriched-enrolment randomised withdrawal study. *EClinicalMedicine* **59**, 101971 (2023).
44. A. Dormer, M. Narayanan, J. Schentag, D. Achinko, E. Norman, J. Kerrigan, G. Jay, W. Heydorn, A review of the therapeutic targeting of SCN9A and $Na_V1.7$ for pain relief in current human clinical trials. *J. Pain Res.* **16**, 1487–1498 (2023).
45. D. A. Eagles, C. Y. Chow, G. F. King, Fifteen years of $Na_V1.7$ channels as an analgesic target: Why has excellent in vitro pharmacology not translated into in vivo analgesic efficacy? *Br. J. Pharmacol.* **179**, 3592–3611 (2022).
46. K. Kingwell, $Na_V1.7$ withholds its pain potential. *Nat. Rev. Drug Discov.* **18**, 321–323 (2019).
47. J. V. Mulcahy, H. Pajouhesh, J. T. Beckley, A. Delwig, J. du Bois, J. C. Hunter, Challenges and opportunities for therapeutics targeting the voltage-gated sodium channel isoform $Na_V1.7$. *J. Med. Chem.* **62**, 8695–8710 (2019).
48. G. Goodwin, S. B. McMahon, The physiological function of different voltage-gated sodium channels in pain. *Nat. Rev. Neurosci.* **22**, 263–274 (2021).
49. J. C. Chambers, J. Zhao, C. M. N. Terracciano, C. R. Bezzina, W. Zhang, R. Kaba, M. Navaratnarajah, A. Lotlikar, J. S. Sehmi, M. K. Kooner, G. Deng, U. Siedlecka, S. Parasramka, I. El-Hamamsy, M. N. Wass, L. R. C. Dekker, J. S. S. G. de Jong, M. J. E. Sternberg, W. McKenna, N. J. Severs, R. de Silva, A. A. M. Wilde, P. Anand, M. Yacoub, J. Scott, P. Elliott, J. N. Wood, J. S. Kooner, Genetic variation in SCN10A influences cardiac conduction. *Nat. Genet.* **42**, 149–152 (2010).
50. R. Coppini, C. Ferrantini, $Na_V1.8$: A novel contributor to cardiac arrhythmogenesis in heart failure. *Cardiovasc. Res.* **114**, 1691–1693 (2018).
51. A. O. Verkerk, C. A. Remme, C. A. Schumacher, B. P. Scicluna, R. Wolswinkel, B. de Jonge, C. R. Bezzina, M. W. Veldkamp, Functional $Na_V1.8$ channels in intracardiac neurons: The link between SCN10A and cardiac electrophysiology. *Circ. Res.* **111**, 333–343 (2012).
52. J. Hordeaux, E. L. Buza, C. Dyer, T. Goode, T. W. Mitchell, L. Richman, N. Denton, C. Hinderer, N. Katz, R. Schmid, R. Miller, G. R. Choudhury, M. Horiuchi, K. Nambiar, H. Yan, M. Li, J. M. Wilson, Adeno-associated virus-induced dorsal root ganglion pathology. *Hum. Gene Ther.* **31**, 808–818 (2020).
53. C. G. Faber, J. G. J. Hoeijmakers, H. S. Ahn, X. Cheng, C. Han, J. S. Choi, M. Estacion, G. Lauria, E. K. Vanhoutte, M. M. Gerrits, S. Dib-Hajj, J. P. H. Drenth, S. G. Waxman, I. S. J. Merkies, Gain of function $Na_V1.7$ mutations in idiopathic small fiber neuropathy. *Ann. Neurol.* **71**, 26–39 (2012).
54. M. S. Minett, M. A. Nassar, A. K. Clark, G. Passmore, A. H. Dickenson, F. Wang, M. Malcangio, J. N. Wood, Distinct $Na_V1.7$-dependent pain sensations require different sets of sensory and sympathetic neurons. *Nat. Commun.* **3**, 791 (2012).
55. C. P. Regan, P. Morissette, R. L. Kraus, E. Wang, L. Arrington, M. Vavrek, J. de Hoon, M. Depre, T. Lodeweyck, I. Demeyer, T. Laethem, A. Stoch, A. Struyk, Autonomic dysfunction linked to inhibition of the $Na_V1.7$ sodium channel. *Circulation* **149**, 1394–1396 (2024).
56. K. Bey, J. Deniaud, L. Dubreil, B. Joussemet, J. Cristini, C. Ciron, J. Hordeaux, M. Le Boulc'h, K. Marche, M. Maquigneau, M. Guilbaud, R. Moreau, T. Larcher, J. Y. Deschamps, M. Fusellier, V. Blouin, C. Sevin, N. Cartier, O. Adjali, P. Aubourg, P. Moullier, M. A. Colle, Intra-CSF AAV9 and AAVrh10 administration in nonhuman primates: Promising routes and vectors for which neurological diseases? *Mol. Ther. Methods Clin. Dev.* **17**, 771–784 (2020).
57. O. J. Yang, G. L. Robilotto, F. Alom, K. Alemán, K. Devulapally, A. Morris, A. D. Mickle, Evaluating the transduction efficiency of systemically delivered AAV vectors in the rat nervous system. *Front. Neurosci.* **17**, 1001007 (2023).
58. S. Blackshaw, Why has the ability to regenerate following CNS injury been repeatedly lost over the course of evolution? *Front. Neurosci.* **16**, 831062 (2022).
59. W. Cai, J. Cao, X. Ren, L. Qiao, X. Chen, M. Li, W. Zang, shRNA mediated knockdown of Nav1.7 in rat dorsal root ganglion attenuates pain following burn injury. *BMC Anesthesiol.* **16**, 59 (2016).
60. J. Pan, X. J. Lin, Z. H. Ling, Y. Z. Cai, Effect of down-regulation of voltage-gated sodium channel Nav1.7 on activation of astrocytes and microglia in DRG in rats with cancer pain. *Asian Pac. J. Trop. Med.* **8**, 405–411 (2015).
61. C. Rinaldi, M. J. A. Wood, Antisense oligonucleotides: The next frontier for treatment of neurological disorders. *Nat. Rev. Neurol.* **14**, 9–21 (2018).
62. Y. Chu, R. T. Bartus, F. P. Manfredsson, C. W. Olanow, J. H. Kordower, Long-term post-mortem studies following neurturin gene therapy in patients with advanced Parkinson's disease. *Brain* **143**, 960–975 (2020).
63. P. Hadaczek, J. L. Eberling, P. Pivirotto, J. Bringas, J. Forsayeth, K. S. Bankiewicz, Eight years of clinical improvement in MPTP-lesioned primates after gene therapy with AAV2-hAADC. *Mol. Ther.* **18**, 1458–1461 (2010).
64. E. A. Paterson, P. V. Turner, Challenges with assessing and treating pain in research primates: A focused survey and literature review. *Animals (Basel)* **12**, 2304 (2022).
65. K. Gomez, H. J. Stratton, P. Duran, S. Loya, C. Tang, A. Calderon-Rivera, L. François-Moutal, M. Khanna, C. L. Madura, S. Luo, B. McKiver, E. Choi, D. Ran, L. Boinon, S. Perez-Miller, M. I. Damaj, A. Moutal, R. Khanna, Identification and targeting of a unique $Na_V1.7$ domain driving chronic pain. *Proc. Natl. Acad. Sci. U.S.A.* **120**, e2217800120 (2023).
66. N. Kusunose, S. Koyanagi, K. Hamamura, N. Matsunaga, M. Yoshida, T. Uchida, M. Tsuda, K. Inoue, S. Ohdo, Molecular basis for the dosing time-dependency of anti-allodynic effects of gabapentin in a mouse model of neuropathic pain. *Mol. Pain* **6**, 83 (2010).

Acknowledgments: We thank Y. Santiago for primary neuron culture and D. Chung for help with Affymetrix analysis. We thank C. Gasper for facilitating the animal studies, A. Ledeboer for reviewing animal protocols, and J. Perez for biorepository of animal samples. We thank S. Xie and N. Yan from AfaSci (Redwood City, CA, USA) for conducting the SNI mouse study and individuals at Charles River Laboratories (Reno, NV, USA) for conducting the NHP study. We thank T. Fieblinger, G. Cisbani, and F. Peters at Evotec (Hamburg, Germany) for conducting single-cell RNAscope analysis on mouse tissues and L. Chatelain and F. Li from ACD (Newark, CA, USA) for conducting single-cell RNAscope analysis on NHP tissues. We thank A. Resch and J. Shoffner for helpful discussions. We thank A. Young, G. Davis, G. Brasnjo, E. McNeil, L. Wilkie, N. Dubois-Stringfellow, P. Ramsey, and A. Resch for reviewing the manuscript. **Funding:** All studies were funded by Sangamo Therapeutics. **Author contributions:** M. Samie, B.Z., J.F., and A.P. devised the program and the main conceptual ideas and proof outline. K.M. and TP designed and managed animal (mouse and NHP) studies. J.E. designed the ZFR library, with input from M. Samie and B.Z. M. Samie designed and managed the in vitro studies with input from B.Z. and A.P.

P.D. and J.L. performed and analyzed the high-throughput screen in neuronal cell lines. P.D., J.L., and D.B.V. performed Affymetrix analysis in primary neurons. M.J. performed gene expression and neuronal firing experiments in primary neurons, and M. Samie analyzed and interpreted the data. T.P. and K.K. managed mouse studies at the CRO (AfaScie Inc.). M.J. processed the tissues and performed gene expression experiments; M. Som analyzed and interpreted the data. M. Samie and B.Z. managed the single-cell data analysis on mouse tissues at the CRO (Evotec). T.P. and K.K. managed NHP studies at the CRO (Charles River Laboratories). J.H., B.J., and M.F. processed the tissues, performed gene expression experiments, and analyzed the data. T.P. worked with the pathologies at the CRO to analyze the NHP safety data (clinical pathologist and tissue histopathology). K.M. oversaw all the NHP data analysis. Y.P. and Y.L. managed the single-cell data analysis on NHP tissues at the CRO (ACD). S.H. managed the synthesis and production of the ZFR library. A.G., T.C., S.B., and A.W. manufactured and analyzed materials for mouse studies. M.T., A.C., and M. Som manufactured and analyzed materials for NHP studies. S.Y. led the manufacturing process, formulation, and analytical development and subsequent at-scale manufacturing to produce the material used in the study. M. Samie wrote the manuscript and made the figures with input from all authors. **Competing interests:** M. Samie and J.E. are inventors on a pending US patent application related to this work titled "Zinc Finger Protein Transcription Factors for the Repressing Nav1.7 Expression" (WO 2024/220578 A2). M. Samie, J.L., P.D., J.E., Y.P., M.F., S.H., T.C., S.B., M.T., A.C., M. Som, Y.L., S.Y., K.M., and B.Z. are current employees of Sangamo Therapeutics Inc. M.J., D.B.V., J.H., B.J., T.P., A.W., J.F., and A.P. were employed by Sangamo Therapeutics Inc. when this work was conducted. **Data, code, and materials availability:** All data associated with this study are present in the paper or the Supplementary Materials. All materials newly generated in this study are commercially available or will be available upon reasonable request from the corresponding author at Sangamo Therapeutics.

Submitted 21 October 2024
Resubmitted 21 October 2025
Accepted 20 February 2026
Published 25 March 2026
10.1126/scitranslmed.adu0217

Science Translational Medicine

Engineered zinc finger repressors induce a prolonged and selective repression of *SCN9A* in nociceptors of nonhuman primates

Mohammad Samie, Toufan Parman, Mihika Jalan, Jisoo Lee, Patrick Dunn, Jason Eshleman, Dianna Baldwin Vidales, Kenneth Kennard, Josh Holter, Brian Jones, Yonghua Pan, Marina Falaleeva, Sarah Hinkley, Alicia Goodwin, Tammy Chen, Sumita Bhardwaj, Alex Ward, Michael Trias, Anthony Chikere, Madhura Som, Yanmei Lu, Sandeep Yadav, Jason Fontenot, Bryan Zeitler, Amy Pooler, and Kathleen Meyer

Sci. Transl. Med. **18** (842), eadu0217. DOI: 10.1126/scitranslmed.adu0217

Editor's summary

The voltage-gated sodium channel Nav1.7 is critical for peripheral pain signaling, but the development of safe small-molecule inhibitors has been challenged by structural similarities between Nav1.7 and other Nav channels. Here, Samie *et al.* designed zinc finger repressors (ZFRs) to selectively bind and repress the expression of Nav1.7 encoded by the *SCN9A* gene. ZFR-mediated repression of the target gene inhibited pain-related behaviors in a mouse model of neuropathic pain and reduced Nav1.7 function in iPSC-derived human neurons. Intrathecal injection of an AAV vector carrying a ZFR targeting human *SCN9A* (ST-503) led to persistent and selective repression of SCN9A in the dorsal root ganglia of cynomolgus monkeys without dose-limiting toxicity or cardiac issues. These data support the clinical development of ST-503, which will be evaluated in a phase 1 clinical trial in patients with idiopathic small fiber neuropathy, NCT06980948. —Daniela Neuhofer

Science Translational Medicine (ISSN 1946-6242) is published by the American Association for the Advancement of Science. 1200 New York Avenue NW, Washington, DC 20005. The title *Science Translational Medicine* is a registered trademark of AAAS.